Department of Precision and Microsystems Engineering

Strategies for precision adhesive bonding of optical micro-components

Pieter-Bas de Potter

Report no : 2024.058
Professor : Dr. ir. M. (Marcel) Tichem
Specialisation : Micro and Nano Engineering
Type of report : Master Thesis
Date : 19 July 2024

TU Delft Delft University of Technology

Challenge the future

Strategies for precision adhesive bonding of optical micro-components

by

Pieter-Bas de Potter

to obtain the degree of Master of Science
at the Delft University of Technology,
to be defended publicly on Tuesday August 20, 2024 at 2:30 PM.

Student number: 4911261
Project duration: September 12, 2023 – August 20, 2024
Thesis committee: Dr. ir. M. (Marcel) Tichem, TU Delft, supervisor
M.K. (Murali) Ghatkesar, TU Delft

TU Delft

Abstract

This study establishes an adhesive bonding strategy for the micro-assembly of optical components using UV-curable adhesives. The focus is on factors influencing adhesive shrinkage and alignment accuracy. Key findings reveal that higher UV intensity reduces both volumetric and linear shrinkage, while curing from below the substrate minimizes horizontal shifts on the to-be bonded optical components, eliminating the need for horizontal offset adjustments. The study highlights how variations in the distance between the substrate and component affect vertical shrinkage displacements and stresses the importance of precise adhesive volume control to enhance accurate shrinkage prediction. The developed shrinkage prediction model forecasts sub-micrometer accurate vertical component shrinkage compensations, validated through comprehensive parameter testing. To advance research toward more accurate shrinkage predictions and a deeper understanding of adhesive shrinkage behavior, future studies propose integrating multi-angle observation systems and expanding parameter testing. These efforts aim to refine prediction models and validate strategies in real-world applications, thereby enhancing the reliability and precision of optical systems across industrial and scientific domains.

Preface

My fascination with assembly and micro-assembly has driven my academic pursuits. This intrinsic interest, coupled with the desire to understand unknown adhesive behaviors, motivated me to undertake this Master's Thesis. Through hands-on testing, I was able to gain a deeper understanding of micro-engineering and its complexities. This experience has been invaluable, as it provided me with practical insights and a tangible sense of the challenges and nuances involved in this field. The ultimate goal of my work was to drive innovation in medical devices, contributing to more successful surgeries and better patient outcomes.

I want to thank several individuals who played pivotal roles in my journey. Marcel Tichem, your critical insights, timely pushes, enthusiasm, and motivation guided me toward finding my own path and successfully achieving the main research goal. Zohreh Farmani, your support during the initial stages of the research, when I felt a bit lost, provided me with much-needed comfort and reassurance. Your reassurance that feeling a bit lost is part of the process was immensely comforting and helped me persevere. Murali Krishna Ghatkesar, thank you for helping me navigate the complexities of adhesive dispensing and selection, and for your valuable insights into potential solutions for this challenging problem.

I would like to extend my gratitude to Alex van den Bogaard, Bradley But, and Rob Luttjeboer from the PME lab team. Thank you for guiding me in the proper testing methods and necessary practical skills.

Thank you to everyone who has supported me throughout this journey. Your contributions have been crucial for the completion of this project. Finally, I would like to thank the committee in advance, for dedicating time to review this thesis and participate in the defense. Your commitment is greatly valued.

Pieter-Bas de Potter
Delft, July 2024

Contents

1 Introduction

1.1. Background

Endoscopic probes have emerged as critical tools in modern healthcare, revolutionizing the way clinicians diagnose and visualize various medical conditions. These instruments, with their slender and advanced imaging capabilities, have opened up new frontiers in minimally invasive surgery (MIS), enabling healthcare professionals to assess the innermost regions of the human body with outstanding precision and minimal disruption to the patient's body [1].

The assembly of endoscopic probes is a complex and multifaceted process that lacks a standardized framework. In the pursuit of developing cutting-edge probes that meet the strict functional requirements essential for their intended medical applications, there is often a tendency to prioritize functionality over the difficulty of the manufacturing process. This approach can lead to challenges in achieving consistent and efficient assembly, as the difficulties of design and manufacturing are conflicting. Thus requiring careful consideration and alignment to optimize both performance and production.

In the construction of endoscopic probes, a crucial phase involves the integration and joining of various components within the probe housing. In many instances, this integration is achieved through a fully manual assembly process [2] [3]. Given that the performance of endoscopic probes depends on the impeccable alignment of their optical parts, it is of vital importance to employ reliable assembly and joining techniques to ensure the optimal functionality of the endoscopic probes.

Endoscopic instruments encompass a wide array of endoscopic modalities. Within this wide array of modalities, three modalities are based on different working principles while utilizing similar components to function well as endoscopic probes. These modalities are ultrasound (US) imaging which utilizes sound waves to create images [4], photoacoustic (PA) imaging which creates an image by using the different light absorption properties within tissue [5], and lastly, optical coherence tomography (OCT) which has a similar working principle as (US) but it utilizes high-frequency waves to generate a higher imaging resolution [6]. Combinations of these techniques are also possible for the construction of so-called multi-modal endoscopic probes [7].

Understanding endoscopic probes and their overall working principles within the context of these three modalities is important information as the foundation of this research. Within most of the endoscopic probes that use one or a combination of the three modalities, there is a striking similarity between functions and components used, five main functions/components can be identified. These functions encompass: *sending a signal*, which is done by utilizing a fiber. *Focusing of the beam*, which is achieved by using a GRIN (gradient reflective index) lens, used in a design by Ji et al. [8]. *Redirecting the beam*, which is realized by using an angled mirror or prism to reflect the signal by an x amount of degrees so the signal is perpendicular to the longitudinal axis of the probe. *Receiving the signal* which is done by a transducer in the case of US and PA imaging systems. For OCT systems a transducer is not needed since the signal is received by the signal-sending fiber itself as shown with the design

by Wang et al. [9]. Finally, there is the function of *rotating the signal beam*, this is needed because a circumferential scan for imaging is favored. The rotation is realized by integrating micromotors into the design of the endoscopic probe. A design that includes most of these parts can be seen in Figure 1.1 which shows a schematic image of an endoscopic probe designed by Dai et al. [3].

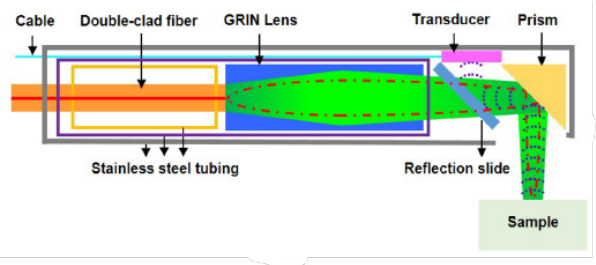

Figure 1.1: Schematic of the probe design by Dai et al. [3], illustrating the five main components housed within the probe.

The manufacturing processes for current cutting-edge endoscopic probes exhibit a notable lack of standardization and consistency. There is no strict assembly process and it is more of a trial-and-error process to realize the designs of the endoscopic probes. However, some categorization can be constructed for the manufacturing ”process” of some endoscopic probes [7]: *manufacturing using tubes and glue* where the probe is manually assembled under a microscope. The tube often has an alignment function like in the design and manufacturing process in [3]. *3D printed manufactured* where the probe housing, designed by Cao et al. [10], was manufactured using micro-resolution stereo-lithography. The last category utilizes a *silicon optical bench (SiOB)* to align the parts of the endoscopic probe, however this results in a cubic shape which enlarges the probe diameter [11].

The absence of standardization and reproducibility in the current manufacturing framework hinders the production of consistent small batches of identical endoscopic probe designs, thereby making commercialization impossible to achieve. This situation is unfortunate, as highly promising designs with the potential to significantly benefit patients may ultimately fail to achieve the status of viable medical instruments for medical practitioners.

Work conducted by Barbara de Vries focuses on the active alignment strategy of the GRIN lens and the optical fiber [12]. An assembly station is constructed and tested to align the GRIN lens within sub-micrometer accuracy. In this research, the GRIN lens is aligned within an open space in the probe housing to coincide with the optical axis of the signal emitted by the fiber, which varies from sample to sample. This situation is illustrated in Figure 1.2, where the yellow part represents the GRIN lens, the pink rod represents the fiber, and the blue part represents the probe housing. The research by Barbara the Vries will be followed up with this research project on how to bond optical micro-components after the alignment process.

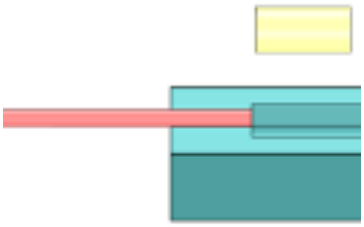

Figure 1.2: Schematic of the fiber/GRIN lens design by Barbara et al. [12], where the pink part indicates the fiber, the yellow cylinder the unaligned GRIN lens, and the blue part the housing.

1.2. Problem statement

This master thesis project is driven by a fundamental challenge in endoscopic probe assembly, particularly the precise joining of optical components to a substrate, within the probe housing, after the alignment process. While reviewing the literature, one main knowledge gap was identified. Existing methodologies for joining optical components encounter limitations in precise alignment and repeatability that hinder the assembly process during the small-batch fabrication of endoscopic probe prototypes. The current bonding method usually consists of dispensing a small volumetric drop of adhesive underneath the GRIN lens which is positioned in a V-groove. Within this process misalignments are not uncommon due to manufacturing tolerances of the V-groove, too much glue being dispensed in the V-groove, and the adhesive shrinkage-induced displacements [13].

By systematically addressing the misalignment issues, caused by the current bonding methods, this research aims to contribute theoretical insights and practical solutions within the field of precise adhesive bonding, specifically for micro-optical components that require accurate alignment. The specific case study for this strategy is the accurate bonding of lenses within endoscopic probe prototypes. This leads to the following main research goal:

"This study aims to develop and evaluate an adhesive bonding strategy for the precise and accurate bonding of optical micro-components."

1.3. Methodology

This section will explain the methodology of this research project where an adhesive bonding strategy is developed and evaluated. The focus of this bonding strategy will be on the case of the GRIN lens within endoscopic probe prototypes. A quantitative research approach is taken to help find the solution to the main research question. This quantitative approach involves the gathering and analyzing of relevant data that gives useful insights into adhesive shrinkage behavior.

The main data that needs to be generated concerns the overall behavior of the UV-curable adhesive, this involves the curing process influences on shrinkage behavior, and the adhesive bond geometry influences on adhesive shrinkage behavior. This specific adhesive-dependent behavior has not been researched in scientific papers that have been reviewed in the literature review [14]. Therefore, this behavior will be analyzed by gathering data through experimental tests conducted using a specialized setup developed to thoroughly examine the previously mentioned aspects of adhesive behavior.

The experimental tests will extract data that provides insights into the substrate-lens distance and dispensed volume influences on the adhesive shrinkage-induced lens movements. The collected data consists of lens displacements, contact angles, and geometrical distances by processing high-quality images that are made during the substrate-adhesive-lens experiments. The image processing is carried out using the ImageJ image processing software. This collected data provides insights into design parameters influencing the alignment accuracies and the repeatability of adhesive bonds, thereby contributing to the development of the final adhesive bonding strategy.

1.4. Structure of the report

To enhance clarity regarding the structure of the paper, this section offers insight into the framework of this Master Thesis report. To start with, Chapter 2 will clarify the required bonding accuracies that the bond strategy aims to accomplish, besides giving insight into UV curable adhesives and their working principles.

The main research goal, as outlined in Section 1.2, encompasses three sub-goals that must be investigated to effectively achieve the primary objective of this research. Chapter 3 will answer these sub-questions. The first sub-goal addressed in Chapter 3, is identifying the most suitable UV-curable adhesive for this bonding strategy, considering crucial performance factors. This is followed by researching the curing influence on adhesive shrinkage, considering the curing speed and curing direc-

tion. The third and final sub-goal involves investigating the effects of the adhesive bond geometry on the adhesive shrinkage behavior, looking into the effects of the lens-substrate height and the dispensed adhesive volume that will form the bond.

Once all these sub-questions have successfully been answered an adhesive bonding test strategy is conducted and explained in Chapter 4. This chapter first elaborates on the overall test strategy procedure, after which all its important steps will be further explained, such as the dispensing process, the shrinkage prediction model, and the curing of the adhesive. The results of the adhesive bonding test strategy will be presented. This chapter will also include findings related to the achieved bond strength.

Chapter 5 provides the ”instruction manual” for the final adhesive bonding strategy. This general strategy provides an overview of important preparations that need to be taken before implementing the bonding strategy into an assembly process. The final adhesive bond strategy steps will also be elaborated. This chapter concludes with the operating requirements for the designed adhesive bonding strategy.

Subsequent chapters, such as the discussion and the conclusions, build upon the results to provide deeper insights, interpretations, and implications for future research or practical applications. Overall, the structure of the Master Thesis paper is designed to systematically address the research goal, from laying the groundwork in the introduction to presenting and analyzing the results in subsequent chapters.

2

Problem analysis

This chapter discusses the alignment requirements for lens bonding to optimize signal transmission. It explores adhesive shrinkage dynamics during curing emphasizing chemical properties. Understanding these factors is essential for developing an effective adhesive bonding strategy capable of achieving precise positioning of optical micro-components.

2.1. Required bond accuracies

The required alignment accuracies for the lens are constructed by Barbara et al. [12]. These alignment accuracies have been constructed through a thorough analysis of the influences of misalignments. Figure 2.1 illustrates the coordinate system of the fiber-GRIN lens assembly. This coordinate system will be consistently utilized throughout the entire research study.

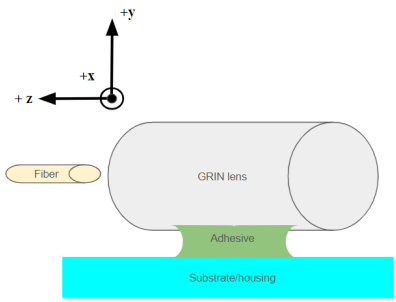

Figure 2.1: Illustration of the GRIN lens, the substrate, and the fiber.

After the lens is aligned, it should be bonded to the housing of the endoscopic probe. Within this research, we will refer to the housing as the substrate. The final positioning of the lens should be within the required alignment accuracies after the shrinkage-induced bonding displacement. The required lens alignment accuracies can be seen in Table 2.1. Achieving these precise alignments ensures optimal light transmission through the lens and fiber assembly. For this research, the same accuracies as constructed by Barbara et al. [7] will be assumed.

The primary goal of this research is not merely to enhance the accuracy of GRIN lens bonding but to establish a comprehensive bonding strategy capable of precisely positioning and bonding various optical micro-components. Given the high precision required in many optical applications, the accuracy requirements for x, y, and z positioning have been made more stringent, with a target accuracy of positioning optical components within 2 [μm]. When positioning the optical component at an angle relative to the substrate, the optical component should not exceed an angular misalignment of 0.23 degrees to maintain the desired component angle and ensure alignment with the optical axis of the signal.

Table 2.1: Required positioning accuracies for both the GRIN lens and the bonding strategy.

Parameter	Required GRIN lens accuracy	Bonding strategy accuracy requirements
δx	3 $[\mu m]$	<2 $[\mu m]$
δy	3 $[\mu m]$	<2 $[\mu m]$
δz	5 $[\mu m]$	<2 $[\mu m]$
Rx	0.23◦	0.23◦
Ry	0.23◦	0.23◦

2.2. Adhesive Shrinkage

This section delves into the intricate interplay between various factors influencing the magnitude and direction of curing-induced adhesive shrinkage. The essence of this phenomenon lies in the chemical properties of the adhesive. Through exploration and analysis, this chapter aims to clarify the dynamics underlying adhesive shrinkage, shedding light on its implications for the construction of the adhesive bonding strategy.

To gain a better understanding of adhesive curing and curing-induced shrinkage, it is beneficial to examine the chemical fundamentals of UV-curable adhesives. A typical UV radiation curing process follows the outline shown in Figure 3.10. A formulation containing photoinitiators, monomers, and oligomers is prepared. This formulation is then dispensed onto a substrate. Upon irradiation, the formulation transforms, forming a solid polymetric tridimensional network, known as a cross-linked polymer. Given the absence of solvents in the UV-curable systems, its key components are the photoinitiator and the monomers and oligomers. The photoinitiator is responsible for light absorption, while the monomers and oligomers are characterized by their functionality to ensure cross-linking polymerization.

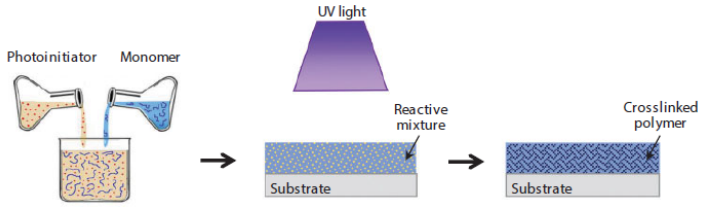

Figure 2.2: UV adhesive formulation and supplementary UV-curing process [15].

Curing processes initiated by irradiation are very fast compared to thermal ones. The curing time can be shortened by increasing the amounts of photoinitiator in the adhesive, and by increasing the light intensity. However, reducing the adhesive curing time to a minimum value is not desirable since extremely fast reactions induced by excessively high UV-light intensity, which is dependent on the adhesive used, can cause poor adhesive performance. The rapid transformation of the liquid adhesive into a polymeric solid network can cause high strain in the polymer, causing a decay in cohesion. Furthermore, the phase transformation comes with a volume contraction called shrinkage [15]. There are two types of shrinkage to consider: volumetric and linear shrinkage.

Volumetric shrinkage is the overall reduction in the volume of the adhesive and results from the chemical reactions during curing. Volumetric shrinkage is particularly challenging in applications requiring high dimensional stability, as it can lead to reduced adhesion and internal stresses [16].

Linear shrinkage is the change in length along any one dimension of the adhesive as it cures. It is important when precise micrometer positioning is required, such as in the bonding of micro-optics or optical fibers. Therefore the main focus of this research will be on linear shrinkage.

3

Adhesive shrinkage research

For the design of the adhesive bonding strategy, experimental tests had to be conducted on the adhesive shrinkage behavior. The existing literature lacks clarity regarding adhesive shrinkage behavior in both the direction and magnitude of shrinkage. In this chapter, an adhesive is selected, the test setup is explained, and the findings from experimental tests on parameters influencing adhesive shrinkage will be discussed.

3.1. Adhesive selection

The adhesive used for bonding the lens within this research is carefully selected. Light-curable acrylics stood out as the best adhesive option, based on their excellent adhesion to glasses, the possibility to cure the adhesive with the use of UV light therefore minimizing the heat that gets into the fragile optical parts, and their rapid full cure time [14]. Three adhesives that suited this research are compared in Table 3.1.

Important performance considerations for a proper comparison are rated for each adhesive. For the assembly of endoscopic probes that need to enter the human body, the ISO 10993 standards should be met. ISO 10993 comprises a series of standards, designed to evaluate the safety of medical devices, aiming to reduce potential biological hazards linked to their use [17]. A low adhesive viscosity is crucial as it enables more precise dispensing of the desired volume.

Table 3.1: A comparison of the adhesives that could be used for the lens bonding, based on case-specific performance considerations.

Performance Consideration (PC)	**Importance rating for PC of adhesive in endoscopic assembly**	**Henkel 3953**	**Henkel 352**	**Viba Uvacryl 2751**
ISO 10993	++	Yes	Yes	No
Elongation at break	-	233%	290%	211%
Low viscosity	++	300-800 mPas	15000-26000mPas	190-300 mPas
Cure type	++	UV-light (365-405 nm)	UV-light (365 nm)	UV-light (320-450 nm)
Full curing time	+/-	30 s	60 s	1-10s point source, 10-60 s UV led
Shrinkage	++	Lin: 2.7%	Unknown	Volumetric: 8% Lin: 2.6%
Adhesion to glasses	++	5 MPa (N/mm^2)	7 MPa (N/mm^2)	9.7 MPa (N/mm^2)

Overall Uvacryl 2751 scores best on most of the adhesive properties. However, since it does not contain the ISO 10993 standards, it cannot be used within endoscopic probes. Therefore this adhesive should not be selected for the actual bonding of endoscopic probe parts that will be used for surgeries.

Upon evaluating two different Henkel adhesives, Henkel 3953 is the preferred choice due to its low viscosity, known linear shrinkage, and strong adhesion to glasses. However, obtaining Henkel 3953

in the short term presents significant challenges, making it impractical for experimental use. Consequently, Viba UVacryl 2751 is selected for this research. Its key characteristics such as viscosity, cure type, and linear shrinkage are similar to those of Henkel 3953. Additionally, Viba UVacryl 2751 is readily available.

3.2. Experimental setup

An experimental setup is designed and assembled to analyze the adhesive shrinkage behavior. This setup had to meet the following requirements:

- Positioning the substrate in z- and x-directions.
- Hold the to-be-bonded object and be able to position it in the y-direction.
- Cure the adhesive from below the substrate.
- Detect the adhesive shrinkage-induced lens shift in the x- and y-direction.
- Make images of the substrate, adhesive bond, and lens before and after curing.

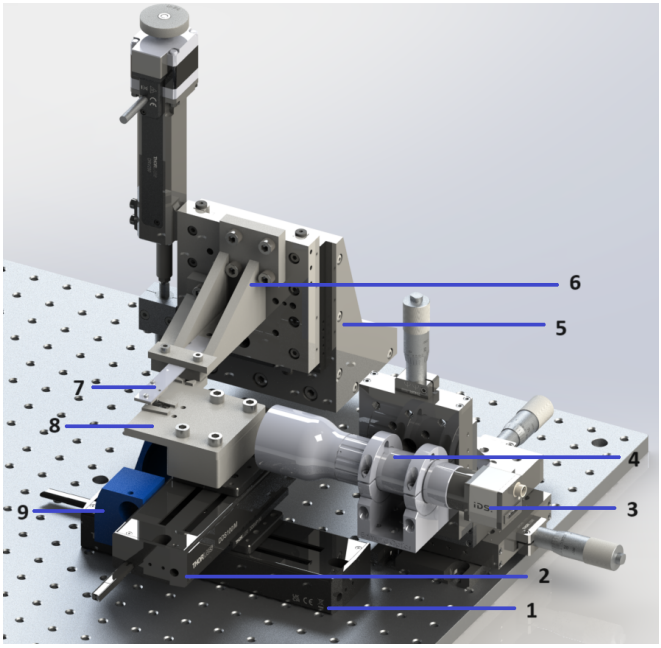

Figure 3.1: Overview of the setup: (1) Linear z-axis translation stage; (2) Linear X-axis translation stages; (3) CCD camera; (4) Telecentric lens; (5) Linear y-axis translation stage; (6) Cantilever beam holder; (7) Cantilever beam; (8) Substrate holder; (9) UV-tunnel.

The setup can be seen in Figure 3.1. A cleaned lens must be attached to the lens holder (7) and a cleaned substrate, with an adhesive drop on top of it, should be attached to the substrate holder (8). The substrate can be moved in the x- and z-directions using positioning stages 1 and 2. The lens can only be moved in the y-direction through the cantilever beam (7) and cantilever beam holder (6), by positioning stage 5. Finally, the adhesive can be cured from below the substrate using a UV-point source and a UV tunnel that reflects the UV light (9). The substrate holder is designed with a hole underneath the substrate so that the UV light can reach the adhesive drop. The cantilever beam holding the lens is designed with a spring stiffness carefully selected to ensure it bends under the adhesive shrinkage-induced forces during the curing process. This is elaborated in Section 3.2.1. A telecentric lens (4), connected to a CCD camera (3) is mounted to an x-y-z positioning stage that can position the focus point of the camera and lens to the desired location. Figure 3.2 shows the rear view of the setup, where the yellow beam indicates that the UV waves are reflected by the mirror towards the substrate, enabling UV curing from below.

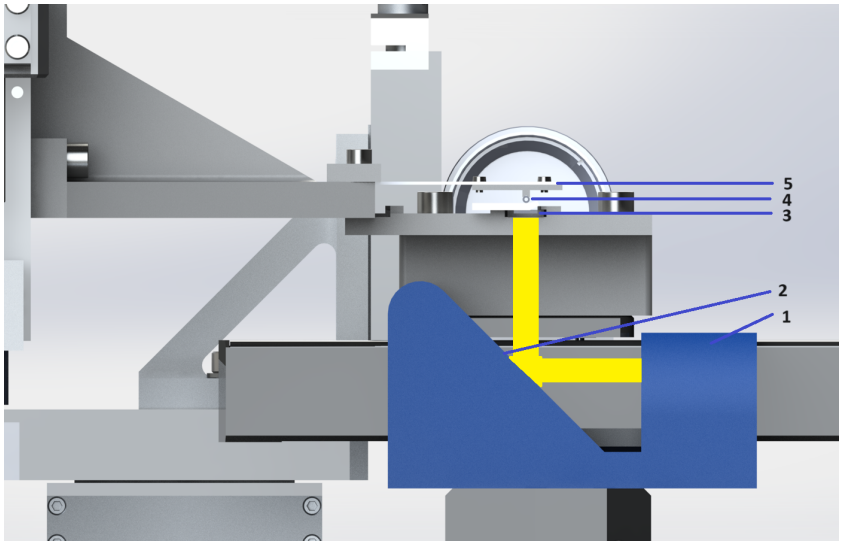

Figure 3.2: Rear view of the setup: (1) UV tunnel; (2) Mirror; (3) substrate; (4) Lens; (5) Lens holder.

3.2.1. The cantilever beam lens holder

The mechanical connection between the object to be bonded and the positioning stage is realized by a steel spring. This steel spring, connected to the position stages, is a cantilever beam. Its spring constant is carefully selected such that the spring force is larger than the viscosity force of the uncured adhesive, at the same time the spring force should be smaller than the shrinkage force.

The viscosity force can be calculated with Formula 3.1. For the tests that are conducted the stage speeds do not exceed 4 mm/s. The maximum viscosity force that the object, and therefore the cantilever beam, will face is $4 \cdot 10^{-9}[N]$. This viscosity force will be selected as the minimum force for the spring constant of the cantilever beam such that the beam will not be deflected when carefully manipulating the object once it is in contact with the adhesive on top of the substrate.

$$F_{viscous} = \eta \cdot A \cdot \frac{du}{dy} \tag{3.1}$$

Where:
$F_{viscous}$ = viscous force [N]
η = dynamic viscosity of the fluid [$Pa \cdot s$]
A = area on which the fluid is connected to the lens [m^2]
$\frac{du}{dy}$ = velocity gradient [m/s]

Based on the research conducted by Pires et al. [18] it is estimated that the shrinkage force is 2 N/mm^2. The contact area of the lens that is in contact with the adhesive depends on the adhesive's wettability on the lens, the height between the lens and the substrate, and the adhesive drop volume. The lowest contact area found was for the maximum gap height of 200 with a contact area of 1.72 [mm^2]. This gives a total Shrinkage force of 3.44 [N]. This minimum "shrinkage" force was selected and rounded down as the maximum force for the spring constant of the cantilever beam, being 3 [N] coming down to a spring constant of 3 [N/mm]. With these spring force boundaries, a cantilever beam dimension was designed. H&S precision Gauge is used as the cantilever beam. Its dimensions were calculated using the Matlab code, see appendix A. The dimensions measure 51.9 [mm] in length, 12.7 [mm] in width, and 0.85 [mm] in height.

3.2.2. Lens and substrate fixation methods

The fixation of both the lens and substrate needs to be rigid to prevent any unwanted movements relative to the lens and substrate holder. This stability is crucial when observing the adhesive behavior and shrinkage-induced lens displacements.

The lens is pushed into a V-groove by the lens-fixation beam. The force exerted by the beam on the lens can be increased by tightening the bolt as shown on the right side of Figure 3.3. The lens holder is bolted onto the cantilever beam and still provides the right spring flexibility since it still properly bends under the adhesive curing forces. The substrate is attached by using two sliding slots on the left and right sides of the substrate, as can be seen in Figure 3.4. This fixation method proved to be sufficiently rigid to keep the substrate in place. Note that there is an opening beneath the substrate to allow UV light to reach the adhesive from below.

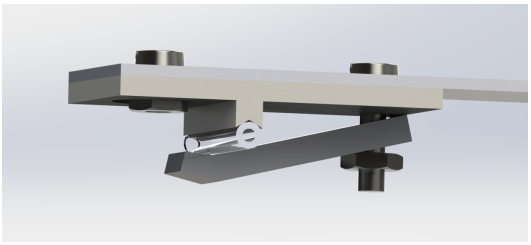

Figure 3.3: Lens fixation method, where the lens is pushed into a v-groove, connected to the cantilever beam.

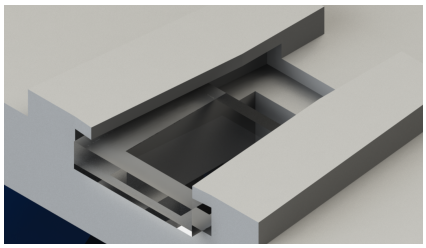

Figure 3.4: Substrate fixation method illustrating the glass substrate secured by two sliding slots.

3.2.3. Data extraction

To extract the desired data, images are taken with an IDS U3-3080CP-C-HQ rev2.2 CCD sensor [1]. This sensor has a resolution of 2448x2048 (h x v), an optical area of 8.446 x 7.066 [mm], and a pixel size of 3.45 [μm]. A 2X magnification telecentric lens is mounted on the sensor to reduce the optical area to 4.223 x 3.533 [mm] and the pixel size to 1.725 [μm], allowing for more accurate measurements.

Pixel-to-real-life dimension conversion using a telecentric lens ensures consistent and accurate measurements. Since the telecentric lens maintains a constant field of view (FOV) regardless of the object's distance from the lens, the magnification factor remains fixed. In our system, this fixed magnification translates to a consistent pixel size of 1.725 [μm]. To perform the conversion, the imaging system was first calibrated by capturing the lens as a reference object with known dimensions under the same imaging conditions. This calibration allowed determining the exact relationship between pixel counts in the image and real-world measurements, eliminating errors due to variations in object positioning within the depth of field (DOF). With this relationship established, any subsequent measurements taken with the telecentric lens can be accurately converted from pixels to micrometers by multiplying the number of pixels by the known pixel size of 1.725 [μm]. This calculation is automated within the image processing software "ImageJ" [2].

When accurately determining a pixel position and pixel displacement between scenarios, five images are taken per scenario. This methodology accounts for the inherent variability and potential slight displacements of pixels in each image, which can occur due to several factors. Firstly, due to the nature of digital imaging, each image captured by the camera can exhibit a minor variation in pixel positioning of the same object, where the pixel grid does not perfectly align with the contours of the object. Furthermore, the camera produces gray areas around the edges of the object due to the interpolation of pixel values, causing slight inaccuracies in determining the exact contour and leading to small positional shifts in each image [19]. By capturing and averaging multiple images, these small variations and displacements can be mitigated, reducing the impact of single image irregularities and leading to a more accurate and reliable determination of pixel positions and displacements. Following the methodology of capturing five images per scenario a measuring inaccuracy of only $\pm$ 0.36 [μm] is achieved. This measurement inaccuracy must be considered when analyzing the data extracted from the captured images.

[1] IDS Imaging Development Systems GmbH, model U3-3080CP-C-HQ, revision 2.2.
[2] ImageJ version 1.53e, developed by the National Institutes of Health, USA, was used for image processing and analysis.

3.3. Curing influence

The curing of the acrylic UV-curable adhesive is a multifaceted process involving several parameters that can be adjusted to control the desired curing rate. The curing speed is dependent on the adhesive and the UV density. The UV density can be adjusted with the following parameters:

- The type of UV-light source
- Light output control
- Distance from the light source
- Temperature and environmental conditions

The parameters, influencing the curing speed, that will be tested on the adhesive bonding of the lens are the light output control and the distance from the light source. These parameters are chosen since they can be adjusted and measured easily. The influence of the curing speed on the shrinkage effects is the primary relationship that is assessed.

The Honle Bluepoint 4 ecocure UV source [3] is used to cure the adhesive. It can emanate multiple wavelengths within the UV wavelength range, thereby changing the light output. The temperature and environmental conditions will not be tested since the setup is located in a lab that does not facilitate reliable environmental condition changes. Tests are done on the same day limiting the changes in environmental conditions from test to test.

The minimum required dose of UV light for the Vibe Uvacryl 2751 is 3000 [mJ/cm^2]. For instance, achieving this dose would necessitate emitting a UV intensity of 50 [mW/cm^2] for 60 seconds. For our curing process different combinations of the curing time, UV intensity, and spot source distance from the source have been selected to influence the curing speed while still providing a minimum required dose of 3000 [mJ/cm^2].

3.3.1. Curing speed experiments

Tests have been conducted with adhesive drops on a transparent substrate. For these tests, the UV intensity was varied over multiple tests to determine the influence of the curing intensity/speed on both the horizontal and vertical linear shrinkage percentage. For these tests, the overall UV dose was constant for every UV intensity cure as explained above. Seven experiments have been conducted for a curing intensity of 60% for 60 seconds with a light source distance of 6 [cm], seven experiments with a 75% UV intensity for 45 seconds with a light source distance of 10 [cm], and seven experiments 100% UV intensity for 24 seconds with a light source distance of 11 [cm].

Figure 3.5 shows the parameters that have been measured from the images. After calibration with the lens, the diameter of the drop was measured by selecting the outer points indicated with the horizontal red line. The determination of the drop height involved marking a horizontal line between the 2 outer points of the drop diameter. This marking allows for a visual indication of the adhesive-substrate interface. The interface is hard to detect from the captured images alone due to the reflectivity of the glass substrate. The drop height and diameter have both been extracted from the uncured and cured drop after which the shrinkage could be determined.

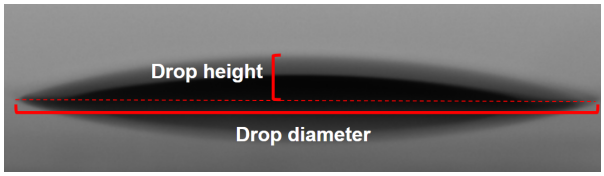

Figure 3.5: Adhesive drop image example, demonstrating the method for measuring drop diameter and height.

[3] Honle UV Technology, Bluepoint 4 ecocure UV source.

From the scatter plot in Figure 3.6, it can be observed that as the UV intensity increases, there is a trend of decreased height shrinkage percentage. This suggests that higher UV intensities lead to less significant shrinkage. The scatter of data points across various droplet volumes indicates that there is variability in the results, but the general trend aligns with the conclusion that higher UV intensities cause less shrinkage. From these test results no strict relation can be found between the shrinkage and the droplet volume.

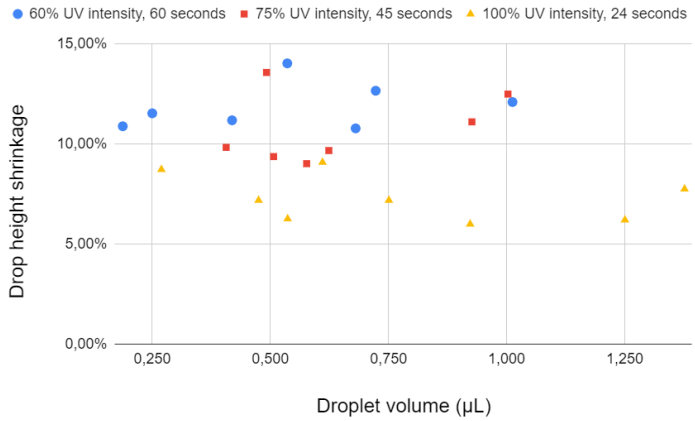

Figure 3.6: Scatter plot showing the relationship between extracted drop height shrinkage percentage, curing intensity, and the estimated droplet volume.

From the plot in Figure 3.7, we can observe that as the UV intensity increases, there also is a trend of decreased diameter shrinkage percentage. This suggests that higher UV intensities lead to less adhesive shrinkage. This relation is mainly noticeable between the 60% UV intensity cures and the 75%, 100% UV intensity cures. No big difference can be observed between the 75% and 100% UV intensity cures.

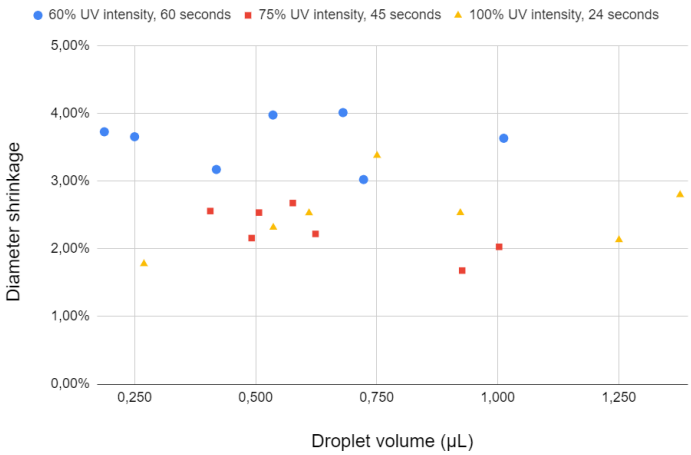

Figure 3.7: Scatter plot showing the relationship between extracted drop diameter shrinkage percentage, curing intensity, and the estimated droplet volume.

The dependency of the adhesive shrinkage on the UV intensity is due to the nature of the curing process. As explained in Section 2.2, UV-light initiates a polymerization reaction causing the adhesive to harden and bond the materials. Lower UV intensity results in slower polymerization reaction rates where the molecules within the adhesive have more time to rearrange and form bonds as they cure, leading to a higher overall shrinkage percentage. Contrary, higher UV intensity accelerated the polymerization reaction, reducing the curing time. Therefore, the molecules in the adhesive have less time to rearrange before the adhesive sets, leading to a reduced shrinkage percentage [20]. The data used to calculate the relevant results can be found in Appendix B, Table B.2.

3.3.2. Curing direction

The adhesive can be cured from different directions. Since the experimental setup blocks light from above the lens, curing was examined from the side of the lens, aligned with the x-axis, and from below the substrate, aligned with the y-axis. The goal of these tests was to determine the effect of the curing direction on the adhesive x-shrinkage effects on the imitator lens. When curing the adhesive from below the substrate, the substrate material should be able to transmit UV waves with wavelengths between 300 and 450 [nm]. The spectral plot in Figure 3.8 shows that fused quartz transmits 93 % of light waves between 280 and 2000 [nm]. Therefore fused quartz is selected as the substrate material.

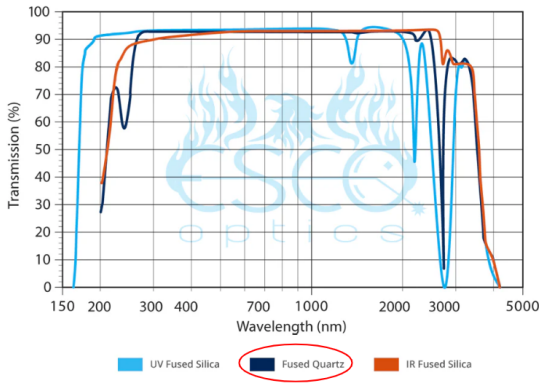

Figure 3.8: Spectral plot of Fused Quartz substrate [21].

The scatter plot in Figure 3.9, shows the x-shift of the lens, caused by the shrinkage of the adhesive on the vertical axis. The horizontal axis represents the gap height at which the test is conducted. The blue dots indicate tests where the adhesive had been cured from below the substrate, and the red triangles show the tests where the adhesive had been cured from above the substrate. This plot gives useful insights into the x-shift of the lens caused by the adhesive, based on the curing direction and the gap height. However, it should be noted that the shift is not always zero when curing from below the substrate. The results also show that the x-shift increases when the gap height increases. Therefore, to minimize the adhesive shrinkage-induced x-shift of the lens, the bond should be cured from below the substrate with a minimum gap height. The used data for these results can be found in Appendix B, Table B.1.

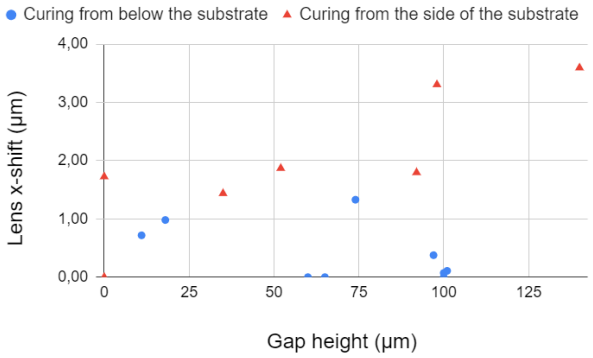

Figure 3.9: Scatter plot showing the relationship between adhesive shrinkage-induced lens x-shift, gap height, and curing direction.

The results show that curing from below gives a reduced x-shift compared to curing from above. The reduced lens x-shift can be explained accordingly: curing from beneath the substrate ensures a uniformly illuminated bond, preventing lens tilts caused by uneven curing along the bond profile, illustrated in Figure 3.10.

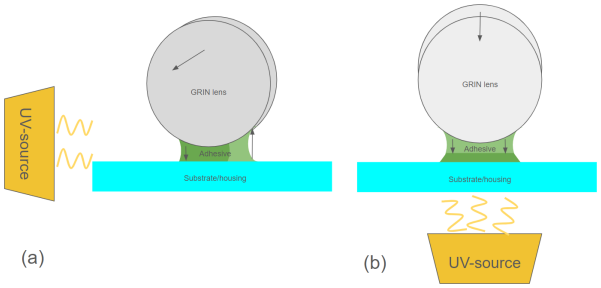

Figure 3.10: (a) Curing from the side of the adhesive drop; (b) Curing from below the adhesive drop.

3.4. Adhesive bond geometry

The geometry of the liquid adhesive was observed using the experimental setup. The adhesive bond geometry is influenced by the following parameters:

- The wettability of the substrate and the lens.
- The adhesive gap height.
- The volume of the adhesive drop.

To determine the influence of each of these three parameters on shrinkage behavior, tests were conducted aiming for individual parameter variations. The following sections detail the testing methods employed and the resulting impacts of each parameter on adhesive shrinkage. These findings form the basis of the shrinkage behavior used to design the adhesive bonding strategy discussed in Chapter 4.

3.4.1. Wettability conditions

The first test data extracted was the wettability of the adhesive on the substrate and the lens individually, and on the final situation when both objects are in contact with the adhesive. The wettability can be described in terms of the contact angle (α) of the adhesive on both parts.

The contact angle formed between the substrate/lens and the adhesive slightly varies per test. The angle can vary based on the cleanliness and surface roughness of the substrate and lens, environmental conditions like humidity and temperature, and the amount of time the adhesive is located on the substrate or lens. Therefore, 10 tests have been conducted to find a proper estimation of the contact angles. The contact angles were measured within ImageJ. Figure 3.11 shows how the contact angle is determined within ImageJ, for the wettability of the substrate. Both of the outer points (1 & 2) of the drop have carefully been selected, after which point 3 is chosen such that line 2 is in contact with the outer surface of the drop.

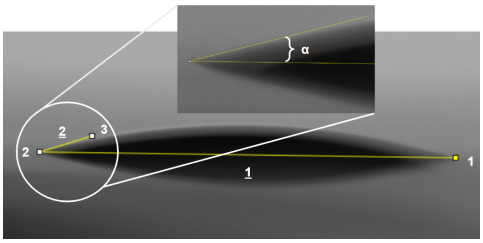

Figure 3.11: Contact angle measurement example in ImageJ, where α indicates the contact angle between the substrate and the adhesive drop.

The average of all contact angles measured during the tests yielded a final value of 15.2 degrees. This wetting situation falls under the category of ”good wetting” since the contact angle is smaller than 90 degrees. This good wettability is desired since it will form a big contact area between the adhesive

and the lens. This results in an increased bond strength compared to the category ”incomplete wetting” where the contact angle is 90 degrees or higher. Ten similar tests have been executed for the contact angle between the lens and the adhesive, the average results from these tests gave a contact angle of 20 [deg]. This also falls in the category of good wetting, allowing for a proper adhesive spread. The wetting angle results subtracted from the test can be seen in Appendix C, Table C.1.

When the adhesive is dispensed on the substrate and the lens is lowered to the position where the adhesive forms a liquid bridge between the two parts, the bond geometry changes from a droplet as shown in Figure 3.11 to a concave meniscus as shown in Figure 3.12. A concave meniscus produces attractive capillary forces that pull the substrate and lens together. This can help to maintain alignment of the optical component [22]. Both α_s ad α_l are below 90 degrees. Again this indicates good wetting of the surfaces by the adhesive. Since the wetting conditions are adequate, no additional steps were taken to enhance wettability through surface treatments.

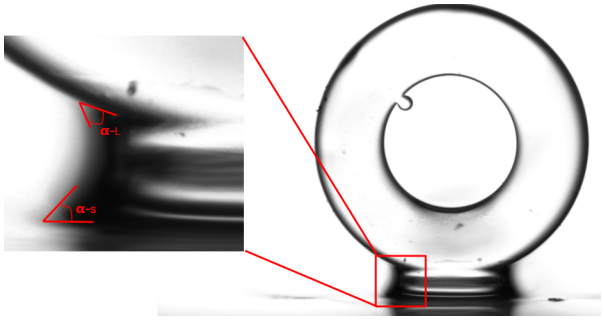

Figure 3.12: Measurement example of substrate-lens bond contact angles, where α_l shows the contact angle between the lens and the adhesive, and where α_s shows the contact angle between the substrate and the adhesive.

3.4.2. Adhesive gap height

The gap height is the distance between the substrate and the lowest part of the lens. Tests were conducted to see the shrinkage effects on the lens for a change in the bond geometry caused by a change in gap height. For these tests, the vertical and horizontal lens displacements were measured using ImageJ.

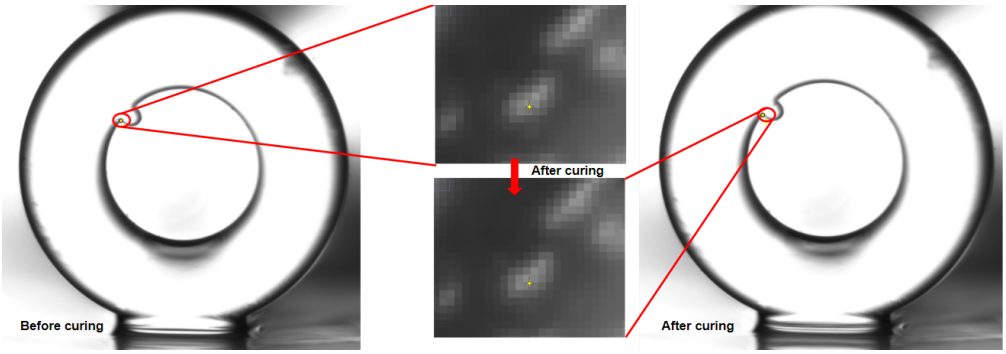

Figure 3.13: Gap height data acquisition method within the ImageJ software. Uncured pixel coordinates (x,y): (1738.69, 1747.59); Cured pixel coordinates (x,y): (1738.75, 1742.36)

25 Tests have been conducted with varying gap heights between 50 and 200 [μm]. To determine the shrinkage of the lens accurately, one recognizable part of the lens image was selected in the form of a pixel, in the images of the substrate-lens bond before curing and the same, but shifted, pixel was selected for the situation after curing, shown in Figure 3.13. By extracting the x- and y-coordinates of these points the vertical and horizontal shift of the lens was calculated.

The gap height has a noticeable influence on the bond geometry. Figures 3.14 and 3.16 show a test with a gap height of 50 [μm], and Figures 3.15 and 3.17 show a test with a gap height of 200 [μm]. The main difference in bond geometry can be seen in the width and length of the adhesive liquid bridge and the contact area between the adhesive and the substrate and lens.

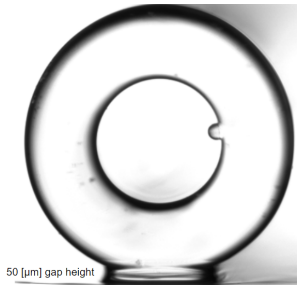

Figure 3.14: Front view of bond geometry 50 [μm] gap height.

Figure 3.15: Front view of bond geometry 200 [μm] gap height.

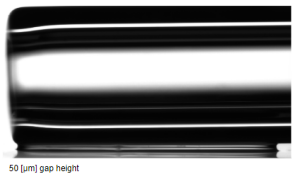

Figure 3.16: Side view of bond geometry 50 [μm] gap height.

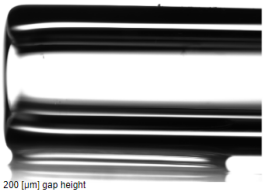

Figure 3.17: Side view of bond geometry 200 [μm] gap height.

The scatter plot shown in Figure 3.18, shows the vertical shift of the lens, caused by the shrinkage of the adhesive on the vertical axis. The horizontal axis shows the gap height. The dispensed adhesive volume in the gap height test results varies between 0.3 and 0.7 [μL] due to the dispensing method, which will be discussed in Section 4.3. This dispensing method cannot consistently dispense a fixed volume of adhesive. Tests that fell within this volume range were analyzed. This range was chosen to prevent the volume-shrinkage influence from having a too dominant effect.

The results show that the absolute y-shift of the lens slightly decreases for an increasing gap height. Therefore, changes in the gap height and consequently bond geometry, influence the linear shrinkage effects on the lens. For larger gaps, the bond is taller, causing the initial shrinkage of the adhesive to pull the uncured liquid adhesive downward first, before affecting the lens position. Conversely, in smaller gaps, the bond is shorter, and the contraction of the uncured adhesive directly impacts the lens alignment more noticeably. This occurs because the adhesive is tightly confined around the bottom of the lens, leading to greater lens contraction. The restricted space in smaller gap heights limits the adhesive's ability to redistribute during curing, intensifying the shrinkage effects on lens positioning.

The data from the plot in Figure 3.18 is used to calculate the percentage of the shrinkage-induced x-shift of the lens relative to the initial gap height. The relationship between this shrinkage percentage and gap height is shown in Figure 3.19. As mentioned before it corresponds with the conclusion that a change in gap height and therefore a change in the bond geometry influence the shrinkage percentage. A power series provides the most accurate prediction of adhesive x-shrinkage across a range of adhesive gap heights.

When looking at the results of the shrinkage-induced x-shift of the lens, shown in Figure 3.20, it can be seen that there are small lens displacements in the x-direction. According to research conducted by [16], for this type of bond geometry with high width/height and length/height ratios, the volumetric shrinkage is mostly confined to the vertical direction of the bond. There is no strict correlation between these x-displacements and the gap height. For these tests, the adhesive is cured from below to reduce

the shrinkage-induced x-shift of the lens as explained in Section 3.3.2. The used data for these results can be found in Appendix C, Table C.2.

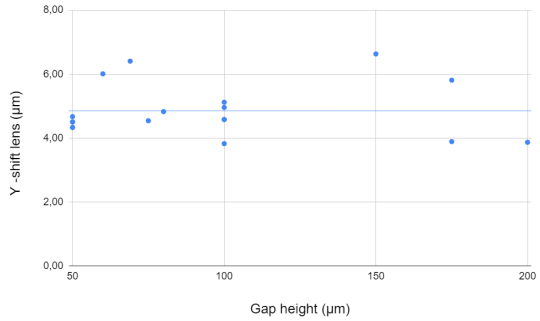

Figure 3.18: Scatter plot showing the relationship between adhesive shrinkage-induced lens y-shift and the gap height, with dispensed adhesive drop volumes between 0.3 and 0.7 [μL].

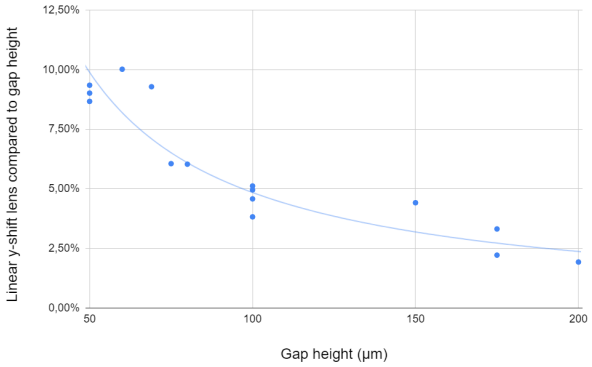

Figure 3.19: Scatter plot showing the relationship between adhesive shrinkage-induced lens y-shift percentage and the gap height, with dispensed adhesive drop volumes between 0.3 and 0.7 [μL].

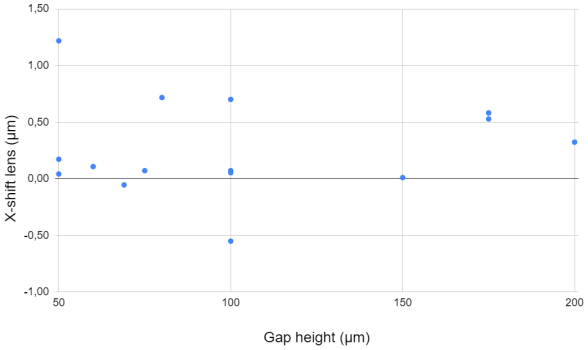

Figure 3.20: Scatter plot showing the relationship between adhesive shrinkage-induced lens x-shift and the gap height, with dispensed adhesive drop volumes between 0.3 and 0.7 [μL], and the adhesive being cured from below the substrate.

3.4.3. Adhesive volume

One of the bond design parameters is the adhesive volume that should be dispensed on the substrate. Changes in the adhesive volume influence the bond strength and the bond geometry. As the adhesive volume increases, so does the contact area between the adhesive and the lens. Figures 3.21 and 3.22 show the observable change in the bond geometry for an increasing adhesive volume. Again the width/height and length/height ratios change for a difference in the dispensed adhesive volume.

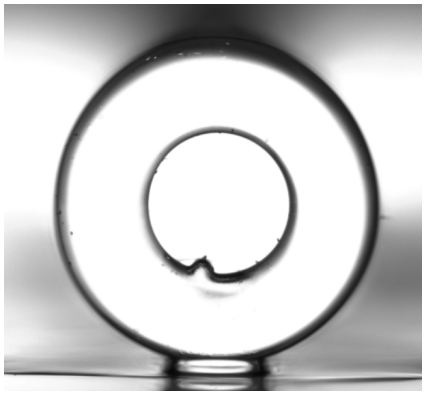

Figure 3.21: Front view of adhesive bond being formed between the substrate and the lens with a 100 [μm] gap height and a drop volume of 0.8 μL.

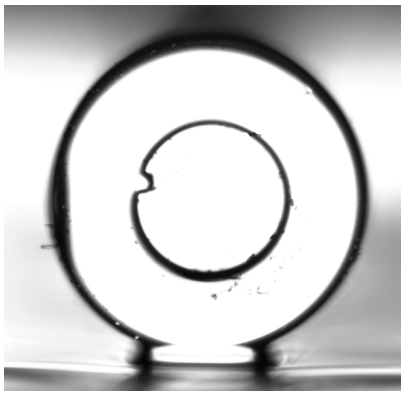

Figure 3.22: Front view of adhesive bond being formed between the substrate and the lens with a 100 [μm] gap height and a drop volume of 1.6 μL.

The relationship between the adhesive-lens contact area and the adhesive volume is derived from the test results shown in Appendix C, Table C.3. The adhesive volume is calculated using the drop shape analysis, using formula 3.2 where the diameter and contact angle of the drop have been extracted from the images, as shown in Figure 3.11. This volume calculation is not precise because the drops are not perfectly round, and the outer contour of the drop is not perfectly spherical.

$$V\,(\theta, r) = \frac{\pi(2 - 3 \cdot cos\theta + cos\theta^3)}{3} \frac{r^3}{sin\theta^3} \tag{3.2}$$

Following this method, the adhesive volume can be indicated. However, this indication is inaccurate, therefore the arc length, which refers to the length of the lens adhesive interface when looking at the front of the lens, is observed since it depends on the adhesive volume. The arc length can be accurately measured, compared to the adhesive volume. Therefore, the relationship between the arc length and the adhesive shrinkage-induced y-shift of the lens will be examined. The arc length provides a useful indication of the adhesive volume. Their correlation is shown in Figure E.2. For an increasing adhesive volume, the arc length increases, as expected.

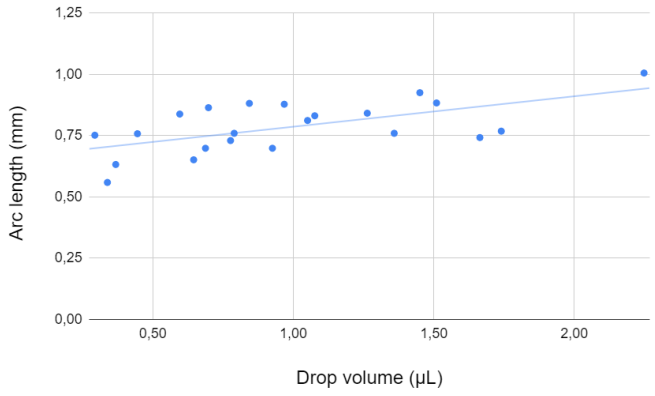

Figure 3.23: Scatter plot showing the relationship between the adhesive-lens arc length and the drop volume.

Besides looking at the geometrical changes of the adhesive bond caused by an adhesive volume change, it is also important to see if drop volume changes cause a change in the shrinkage of the bond. For these tests, the curing intensity and curing direction are kept consistent. Figure 3.24 shows the results from the conducted tests. It is observed that the trend line for vertical lens shrinkage increases

with the rising volume of the adhesive droplet. The results deviate from the trend line since an array of gap heights have been tested.

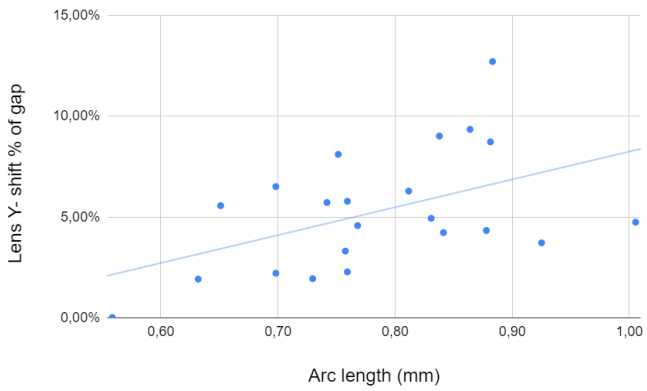

Figure 3.24: Scatter plot showing the relationship between the shrinkage-induced lens y-shift and the adhesive-lens arc length.

This phenomenon can be explained by the theory of surface tension minimization. When a larger volume of adhesive is in contact with the lens, the adhesive spreads over a greater portion of the outer surface of the lens compared to a smaller adhesive drop, given a constant gap height. As the adhesive volume increases, the surface tension drives the adhesive to minimize its surface area, resulting in a more extensive spread over the lens surface. This effect is visually demonstrated in Figure 3.25 a and b, from experimental tests where only the drop volume was changed. The geometry of the bond changes are expressed by the width-height and length- ratios. In Figure 3.25, the red line indicates the bond height, and the blue line the bond width. Therefore, an increase in dispensed volume resulting in increased width-height and length-height ratios leads to a higher adhesive shrinkage-induces lens displacement. This correlation is important for understanding the adhesive's behavior and optimizing the bonding process. Keeping the dispensed volume consistent is preferred when aiming to accurately predict the shrinkage-induced lens y-shift.

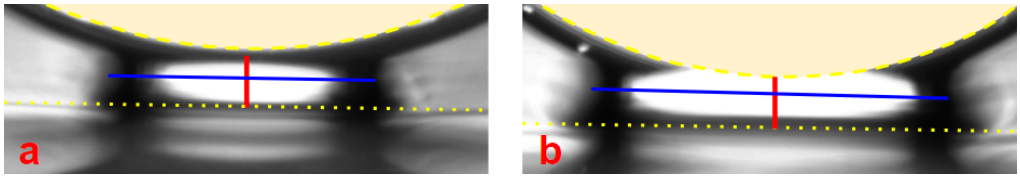

Figure 3.25: (a) Front view of bond geometry formed for a gap height of 50 [μm] and a drop volume of 0.80 [μL]; (b) Front view of bond geometry formed for a gap height of 50 [μm] and a drop volume of 1.60 [μL].

4

Adhesive bonding test strategy: development and results

Based on the adhesive behavior research and results explained in Chapter 3, an adhesive bonding test strategy was designed to evaluate the potential performance. Key aspects include carefully selecting the adhesive, and shrinkage predictions based on the gap height, dispensed adhesive volume, and curing conditions. This chapter begins with an overview of the entire test strategy, followed by a detailed explanation of its key steps. This chapter concludes by showing the accuracy results achieved with the test strategy. This test strategy forms the foundation of the final adhesive bonding strategy discussed in Chapter 5.

4.1. The adhesive bonding test strategy

The adhesive bonding test strategy follows a systematic approach to obtain a reliable sub-2 [μm] precision x and y lens positioning. The process starts with the surface cleaning of the imitator lens and the substrate. The substrate and lens are cleaned with isopropanol to improve the wettability and cleanliness of the surfaces. After the cleaning process, the adhesive is dispensed on top of the substrate, more information about the substrate choice can be found in Section 3.3.2. The adhesive is dispensed using a time/pressure pump dispenser with a gauge 20 UV-blocking nozzle. The adhesive dispensing was conducted safely within a chemical lab due to the health hazards associated with the adhesive. The dispensing method will be further detailed in Section 4.3.

These initial steps are followed by connecting the cleaned lens and substrate to the setup, as explained in Section 3.2.2. When the lens and adhesive are firmly secured the imaging system is calibrated with the lens diameter. After the calibration, images are made from the front side of the lens, making it possible to measure the wall thickness of the glass capillary tubes. This wall thickness is obtained to determine the final gap height. Additionally, images are made of the drop contour. From these images, the drop volume is estimated using drop shape analysis.

Minor differences in how the lens is mounted or how the substrate is placed lead to discrepancies in the baseline gap height measurement, causing the 0 [μm] coordinate to change from sample to sample. Therefore the next step involves lowering the lens with small steps of 2 [μm] until the lens contacts the substrate. This y-coordinate of the y-stage is used in the shrinkage compensation prediction test model. The gap height is put into the prediction test model, which automatically determines the y-coordinate for the y-stage. The initial gap height is checked and adjusted to correct for a 0 [μm] gap height coordinate error caused by the chosen step size and y-stage positioning repeatability.

After the desired gap height is set, the adhesive-lens arc length has to be determined. This arc length represents the length of the adhesive-lens interface as shown in Figure 4.5 and gives an indication of the dispensed volume. If the arc length is within the self-obtained boundaries the test procedure

can continue. If this is not the case the adhesive needs to be cleaned from the lens and the substrate and the test procedure has to start again since the shrinkage test prediction is only valid within these arc length boundaries. If the measured arc length is below the minimum boundary a bigger adhesive volume has to be dispensed, and if the arc length is above the maximum boundary a smaller volume has to be dispensed. A more elaborate explanation of the volume/arc length sensitivity of the adhesive bond strategy is provided in Section 5.3.3.

The shrinkage compensation is calculated in the shrinkage prediction model, this compensation is added to the y-coordinate of the y-stage. Then the adhesive is cured from below with a 100% UV intensity for 24 seconds. More information about the curing process for the designed adhesive bonding test strategy is provided in Section 4.8. The final step of this procedure is checking the final lens positioning. If the x- and y-displacements of the lens position after curing are within 2 [μm] of the desired position, the strategy is completed successfully. The total test procedure is schematically shown in Figure 5.1.

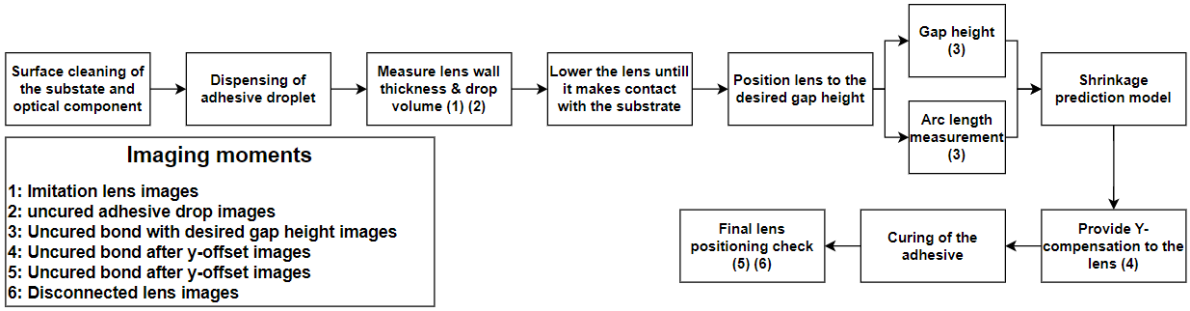

Figure 4.1: Adhesive bonding test strategy process block diagram, with numbers in the blocks corresponding to the image moments explained on the left.

4.2. Test strategy imaging and measurement procedures

Accurate shrinkage prediction and strategy performance require a series of precise imaging steps. The following points provide a detailed explanation of each step in this comprehensive imaging and measurement protocol. The conversion from pixels to micrometers is automatically performed in ImageJ by multiplying the pixel size by the number of measured pixels between image coordinates after the calibration step.

1. **Imitation lens image, Figure 4.2:** From these images the wall thickness of the imitation lens closest to the substrate is extracted. This distance can be measured accurately since the contours of both sections are properly defined. The wall thickness is obtained to calculate the gap height, as discussed in point three. This is essential for this test procedure since the wall thickness of the lens deviates from its specification of 500 [μm]. Based on the data extracted from these images, the wall has an average thickness of 523 [μm] with a standard deviation of 27,82 [μm]. The standard deviation of this thickness is too significant to automatically use the average, as a deviation of 27.82 [μm] can result in an additional shrinkage-induced lens displacement of 1.22 [μm], given a shrinkage percentage of 4.4%.
2. **Uncured adhesive drop image, Figure 4.3:** These images are made to estimate the dispensed adhesive volume. An example of this volume estimation is shown in Figure 3.11.

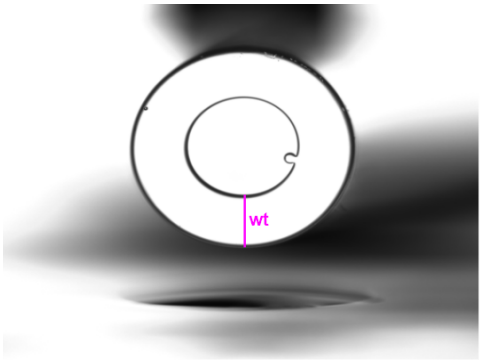

Figure 4.2: Imitation lens example image, with the lens wall thickness indicated by the pink line.

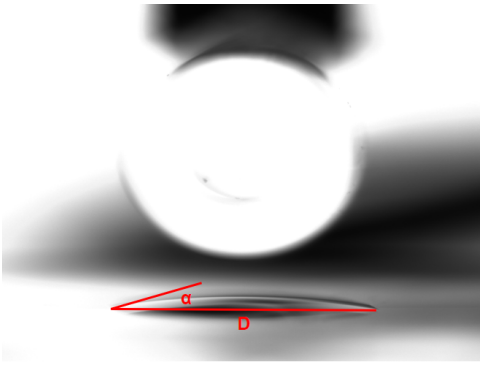

Figure 4.3: Uncured adhesive drop example image, With the horizontal red line indicating the drop diameter and α indicating the contact angle.

3. **Uncured bond with a desired gap height, Figure 4.4:** These images enable verification that the y-axis positioning stage has created the predetermined gap height. The gap height is calculated by subtracting wall thickness (pink line) from the measured distance (orange line). This approach is chosen since it is hard to accurately determine the lowest point of the imitation lens when in contact with the adhesive. These images are also used to check the final lens displacements, by making an image stack with these images and the cured bond after strategy compensation images. In these images angle θ is also extracted, this angle is used to calculate the arc length, indicated by the yellow dashed line.

4. **Uncured bond after strategy compensation, Figure 4.5:** These images are used to check the compensation caused by the y-axis positioning stage. This is necessary for this test procedure since the actual compensation, calculated by the shrinkage prediction model, is not perfectly transferred to the lens by the setup due to the repeatability limitations of the y-stage.

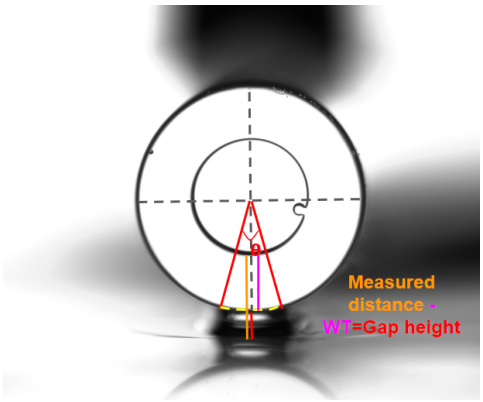

Figure 4.4: Uncured bond with the desired gap height example image, where the gap height is calculated by subtracting the wall thickness from the orange measured distance line. The contact angle is calculated using the lens radius and angle θ.

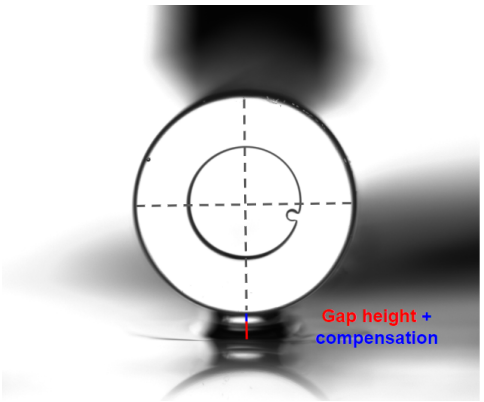

Figure 4.5: Uncured bond after strategy compensation example image, with the blue line indicating the shrinkage compensation.

5. **Cured bond after strategy compensation, Figure 4.6:** As mentioned before, these images are used to determine the lens displacement by comparing them to the uncured bond with desired gap height images.

6. **Cured bond after strategy compensation disconnected from lens holder, Figure 4.7:** The final images that are made are from the cured bond after shrinkage compensation but then disconnected from the lens holder. These images can be compared to the cured bond after strategy

compensation images if the lens is disconnected carefully. Failure to carefully detach the lens causes the entire bonded substrate-lens assembly to shift, hindering accurate image processing comparison. Unfortunately, for the chosen lens connection, disconnecting the lens always resulted in a substrate-lens assembly shift. This disconnecting process should be improved in future work.

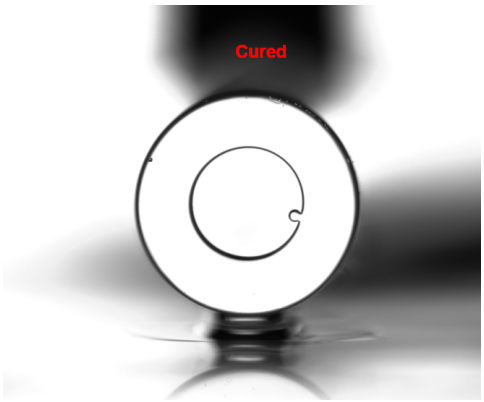

Figure 4.6: Cured bond after strategy compensation example image.

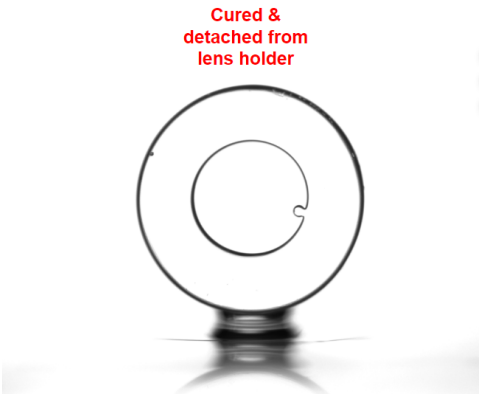

Figure 4.7: Cured bond after strategy compensation disconnected from lens holder example image.

4.3. Dispensing of the adhesive

The dispensing method for this adhesive bond test strategy is realized with the time/pressure DC50 pump system from Fisnar. This system features a precision regulator and a digital pressure gauge to ensure accurate flow control, along with an adjustable vacuum suck-back mechanism to prevent fluid dripping from the dispensing tip. A 20 gauge dosing nozzle was used which has a tip inner diameter of 0.61 [mm]. The nozzle was manually positioned above the center of the adhesive. Automating this process is recommended to eliminate human inaccuracies in the dispensing process.

The regulator was set to 0.006 seconds with an air pressure of 3 bar. These settings proved to dispense an average adhesive volume of 0.87 [μL] with a standard deviation of 0.38 [μL], see Appendix D Table D.1. Based on this deviation, it can be concluded that this dispensing method is insufficient as it fails to accurately dispense an intended volume. The big deviation is likely caused by the compressibility of the air which ”pushes” the syringe plug down allowing the adhesive to get dispensed, air bubbles that form in the adhesive when loading the syringe with the adhesive, and viscosity changes of the adhesive due to temperature variations. Variations in the dispensed adhesive volume affect the shrinkage behavior, resulting in less accurate shrinkage predictions from the shrinkage prediction test model.

4.4. X-offset adhesive-lens placement

Tests have been conducted to observe the adhesive behavior and the shrinkage-induced lens directions and magnitudes when the lens is not perfectly placed above the center of the adhesive drop. An asymmetrical uncured adhesive bond is unwanted since it would result in additional shrinkage-induced lens x-displacements.

An x-offset is created by positioning the Thorlabs x-stage to the left and right, this is shown in Figure 4.8. It can be seen that the lens is positioned to the right relative to the adhesive drop. All conducted tests were given a +600 [μm] or -600 [μm] x-offset. When the lens is lowered to a realistic gap height between 50 and 100 [μm], an almost symmetrical bond forms directly between the lens and the substrate. Figure 4.9 shows an image of the formed bond, where a small difference of 5 [μm] between the middle of the lens and the outer sides of the adhesive bridge was measured.

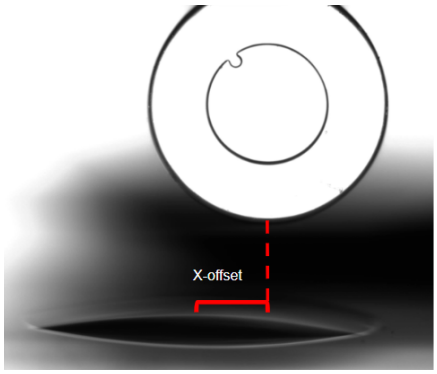

Figure 4.8: Fig: x-offset lens before adhesive-lens contact.

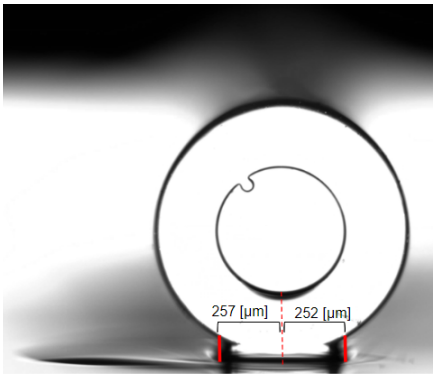

Figure 4.9: x-offset lens after adhesive-lens contact.

The reasoning for this almost symmetrical bond can be explained accordingly. Firstly, the minimization of surface energy drives the liquid adhesive to spread and form a symmetrical shape between the lens and the substrate. A Liquid naturally seeks to minimize its surface area to reduce surface energy, leading it to spread evenly across the available surface. In this case, even if the lens is not perfectly aligned with the adhesive drop, the adhesive still spreads out to form a symmetrical shape between the lens and the substrate. Secondly, the geometry of the lens, particularly its circular shape, plays a role in the formation of the symmetrical liquid bridge. Regardless of the initial alignment, the lowest point of the lens is always closest to the substrate with the adhesive drop on it. This means that the adhesive tends to flow towards the lowest point of the lens, naturally centering itself beneath the middle of the lens. As a result, the adhesive forms a symmetrical bridge, with almost equal amounts of adhesive distributed around the lens. Therefore, the initial horizontal droplet position variation does not affect additional horizontal shrinkage-induced lens shifts.

Four x-offset tests have been conducted, where two tests were dedicated to a right positioning error and two to a left positioning error. The results are shown in Table 4.1. The primary observation from this data, as indicated in the fifth column, is that an x-offset error on both sides does not lead to additional shrinkage-induced x-shift of the lens when compared to tests where the lens is precisely positioned above the drop center as discussed in Section 3.4.2. However, the portion of the total adhesive volume utilized for forming the liquid bridge between the substrate and lens is influenced by an x-offset of the lens compared to proper x-alignment, as some of the adhesive adheres to the substrate, as can be seen in Figure 4.9. This factor impacts the accuracy of volume predictions used to form the liquid bridge between the substrate and the lens, influencing the shrinkage-induced lens shifts. Therefore, it is recommended to align the center of the lens with the center of the adhesive drop.

Table 4.1: Overview of the drop-lens x-offset tests lens shifts results.

Test	**Gap height [μm]**	**Y shift lens [μm]**	**linear Y shrinkage %**	**X shift lens [μm]**
1 Right positioning error	50	2,71	5,41%	0,14
2 Right positioning error	100	3,67	3,67%	0,23
1 Left positioning error	80	4,01	5,02%	0,05
2 Left positioning error	70	2,59	3,70%	0,22

4.5. Z-offset adhesive lens placement

For the z-axis placement between the lens and the adhesive drop, the bond will move to the location with the minimum gap height. Due to the setup's inability to align the lens precisely parallel to the substrate, there is always a small angle difference of around 0.06 [Deg]. However, this angle difference could also occur during the actual assembly of optical components if the optical axis is not aligned parallel to the substrate or housing. The final results concerning the substrate-lens angle and its adhesive behavior can be found in Section 4.9.3.

The bond-forming, based on an angle difference between the substrate and the lens is shown in Figure 4.10 and 4.11. Figure 4.10 shows the lens that is positioned above the adhesive drop before a liquid bridge is formed between the two parts. As can be seen in this figure, the drop is on the left side. When the lens is lowered a liquid bridge is formed and during a few seconds, the liquid walks to the right side of the lens. The bond geometry is in equilibrium at the right side of Figure 4.11 where the substrate-lens gap is the smallest. The final z-placing of the bond is bounded by the outer edges of the substrate or lens.

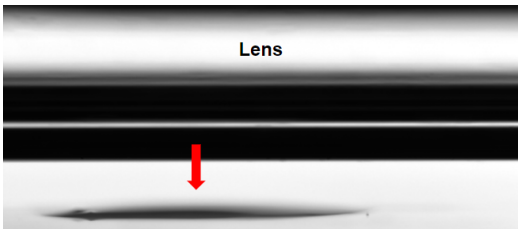

Figure 4.10: Image of adhesive drop location relative to the side of the lens, the red arrow indicates how the lens will be lowered until a liquid bridge is formed between the substrate and the lens.

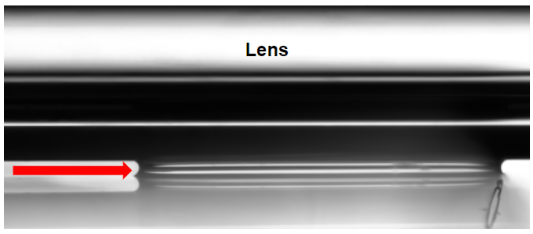

Figure 4.11: Image of the bond formed after the lens contacts the adhesive, with the horizontal red arrow indicating the uncured adhesive drop movement toward the right side of the lens, where the gap height is smallest.

Therefore, in this strategy, the initial placement of the adhesive drop relative to the lens is not critical, as the final liquid bond will shift when there is a slight angle between the substrate and the lens. For the tests that have been conducted with this strategy, the minimum gap height is always at the side where the CCD camera is focused on the lens since the measured gap height is then closest to reality, this is exaggeratedly illustrated in Figure 4.12. If the closest point is on the other side of the lens, furthest away from the CCD camera, a faulty gap height would be measured resulting in unsuccessful tests, this situation is exaggeratedly illustrated in Figure 4.13

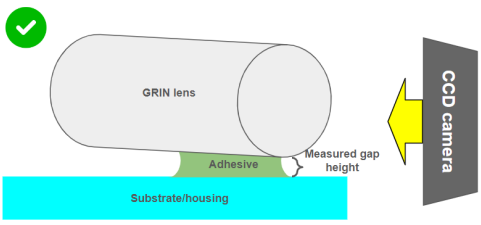

Figure 4.12: Exaggerated illustration of CCD camera placement and desired adhesive bond forming.

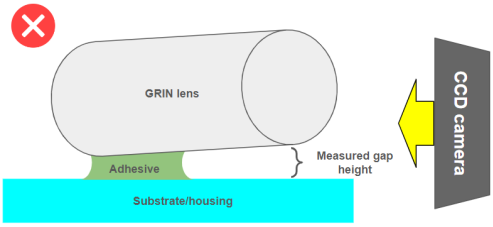

Figure 4.13: Exaggerated illustration of CCD camera placement and undesired adhesive bond forming.

4.6. Shrinkage prediction test models

The shrinkage prediction test model is a self-developed calculator tool that reliably predicts the adhesive shrinkage-induced lens y-shift. This shrinkage prediction can be applied to the lens as a y-compensation adjustment before the adhesive is cured. The shrinkage prediction test model needs the gap height as input. These shrinkage predictions are based on the bond geometry test data. The development of the shrinkage prediction test model has gone through three iterations.

Version 1: Fixed average shrinkage prediction: In this model, an average shrinkage percentage of 4.4% was derived from the preliminary shrinkage results in Section 3.4.2. The V1 shrinkage prediction model did not take the gap height into account. Initially, when testing this prediction model, it looked like it could predict the shrinkage accurately for gap heights between 100 and 150 [μm]. However, when below a gap height of 100 [μm] the final accuracy results showed a slight under-compensation, and when above a gap height of 150 [μm] the final accuracy results showed a slight overcompensation. More research and tests had gone into the gap height influence and an improved prediction model (V2) was developed.

Version 2: Gap-dependent shrinkage prediction: This second version of the shrinkage prediction model used the gap height to calculate the expected adhesive shrinkage-induced lens shift. The data points from Figure 3.19 were used to fit a line that predicts the shrinkage best. A power series line, shown in Equation 4.1 proved to be the best fit for these data points. In Equation 4.1, $P_{y-shrinkage}$ represents the shrinkage percentage and it is dependent on the gap height x. The schematic block diagram of shrinkage prediction model V2 is shown in Figure 4.14. During these tests, the power series was improved by adding the shrinkage results into the line fitting calculation.

$$P_{y-shrinkage} = 5.51x^{-1.03} \tag{4.1}$$

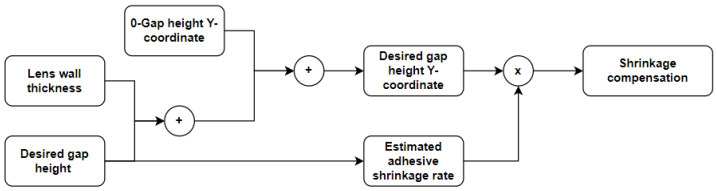

Figure 4.14: V2 compensation prediction model block diagram.

Version 3: Volume- and gap-dependent shrinkage: This final version of the shrinkage prediction test model implemented additional gap height-shrinkage data from version 2 test results, providing an improved fit for the existing data point, as can be seen in Figure 4.15. The final equation that predicts the shrinkage can be seen in Equation 4.2. This final prediction test model also considers the dispensed volume expressed by the arc length.

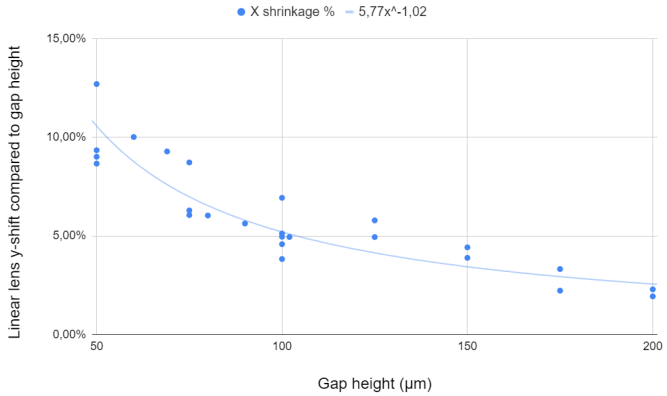

Figure 4.15: Scatter plot indicating the final shrinkage prediction formula depending on the gap height.

Some tests yielded shrinkage results that were marginally different from the predicted shrinkage. After close inspection of the bond geometry, it could be seen that if the arc length was below 0.63 [mm], the actual displacement of the lens was significantly lower than predicted, resulting in a positioning accuracy exceeding 2 [μm]. Conversely, when the arc length exceeded 0.93 mm, the opposite effect was noted. Therefore an additional term "A" was implemented into the V2 test model, finalizing V3 of the

shrinkage prediction test model. This A-term served as a criterion indicating whether the procedure could be continued or not. These arc length boundaries indicate whether the dispensed volume falls within the range where shrinkage compensation can be accurately predicted within 2 [μm].

If the arc length (A_L) is between the just mentioned boundaries: $A = 1$, and if the arc length is outside of the boundaries: $A = -1$. The shrinkage calculation method stays the same however an "if else" statement is added, this is mathematically shown in Equation 4.2. This statement ensures that the test strategy detects a negative shrinkage compensation when the arc length is outside the boundaries, warning the operator to discontinue the test. The schematic block diagram of shrinkage prediction model V3 is shown in Figure 4.16.

$$P_{y-shrinkage} = \frac{5.77x^{-1.02}}{A} \tag{4.2}$$

$$A_L \in [0.63, 0.93] \Rightarrow A = 1$$
$$A_L \notin [0.63, 0.93] \Rightarrow A = -1$$

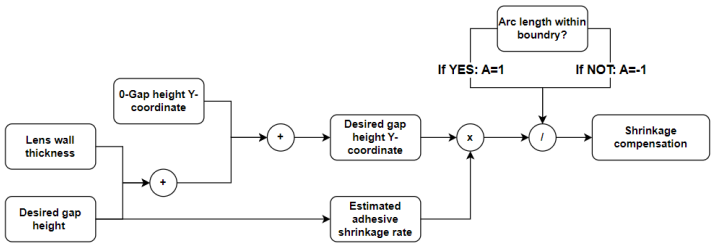

Figure 4.16: V3 compensation prediction model block diagram.

Deviations in the arc length are a result of deviations in dispensed adhesive volume drops. A larger volume causes an increase in shrinkage-induced lens y-displacements. In the experiments performed for this research there existed large volume variations because of limited dispensing resources, this however showed the relevance of dispensing volume control. This volume control should be taken into account for the final shrinkage prediction model, which will be discussed in Section 5.2.

4.7. Positioning stage repeatability y-axis

The Thorlabs DRV250 y-axis positioning stage is crucial for establishing the gap height and compensation. The accuracy and repeatability of the y-stage are not perfect, so its movements have been measured. The initial compensation results can be seen in Appendix D Table D.2. Initially, during the first tests, the compensation error had an average overshoot of + 1.7 [μm], this compensation error was reduced by lowering the maximum y-stage speed from 2 to 0.1 [mm/s], and the acceleration from 2 to 0.01 [mm/s^2]. Under these stage settings, the average compensation error looks sufficiently accurate to meet the accuracy requirements. The maximum compensation error is below the accuracy requirements, so when the shrinkage is accurately predicted the compensation error is sufficiently low to keep the lens positioning within the accuracy requirements during this test strategy process. The final compensation errors can be seen in Appendix D, Table D.3.

4.8. Curing of the adhesive

In Section 3.3, curing tests were conducted. Less shrinkage occurred when the UV intensity was the highest. Therefore a UV intensity of 100% for a duration of 24 seconds and a light source distance of 10 [cm], indicated by the black line in Figure 4.17, was chosen for this test strategy. This light source distance is calculated with equation 4.3, where the light intensity that reaches the adhesive is inversely proportional to the square of the distance. Under these curing parameters, and considering the substrate's 93% transmittance, the adhesive receives the minimum required dose of 3000 [mJ/cm^2], ensuring that it is fully cured.

$$I = \frac{I_0}{d^2} \tag{4.3}$$

The adhesive is cured from below since this results in the most symmetrical curing of the adhesive, favorable when looking at minimizing horizontal shrinkage directions. A UV frame was designed to enable curing from below. This is an essential tool within this setup since the UV spot source laser end was too big to position underneath the substrate with the desired distance. The laser end was connected to the UV frame, and at the end of the frame, a mirror was accurately positioned at 45 degrees such that the UV waves were reflected toward the adhesive. Figure 4.17 shows this tool that allows for curing from below.

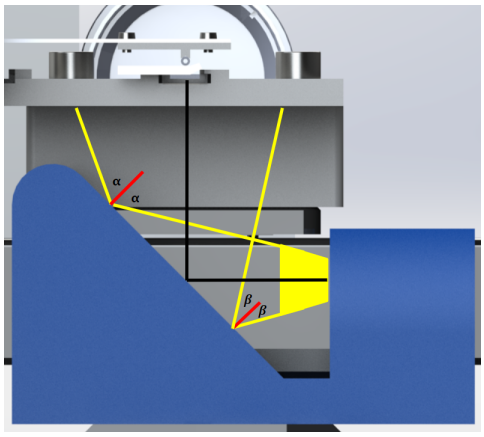

Figure 4.17: Rear view of the setup, illustrating how the UV light is reflected towards the adhesive bond.

4.9. Test results

The adhesive bond test strategy is evaluated throughout its development, and the results are presented in this section. At first, the lateral lens displacement results are examined. This is followed by an analysis of the lens rotation test results. Finally, the repeatability of the test strategy is discussed.

4.9.1. Lateral lens displacements

The objective for the final lateral displacements of the lens after the curing step is to ensure it does not deviate more than 2 [μm] from the target position. The main accuracy concern is in the y-direction since this is the direction in which most of the shrinkage occurs when curing the adhesive from below the substrate.

The performance of the adhesive bonding strategy was evaluated through 21 conducted tests. The results of these tests can be seen in Table 4.2. The first column shows the gap height and its test number. The test numbers highlighted in orange represent prediction model version 2 tests where the shrinkage data was still incorporated into the shrinkage prediction line to improve the shrinkage estimation formula. Consequently, the predicted y-compensation for these tests deviates from the tests indicated in white where the final prediction formula was used. The inclusion of these last shrinkage results only slightly altered the power series formula. Therefore, the integration of new shrinkage data was discontinued.

Two out of the 21 tests, 150 [μm] test 1, and 175 [μm] test 1, resulted in an arc length that was outside of the arc length boundary as stated in Section 5.3.3. These test results provided valuable insights into the arc length requirements for the test strategy. The data underlying these test results were extracted as discussed in Section 4.2. Figure 4.18 shows an exaggerated illustration clarifying columns 4, 5, and 6. Figure 4.19 shows an exaggerated illustration clarifying columns 10, 11, and 12.

The ninth column shows the shrinkage prediction error. Three out of these results are red since these absolute values are above 1.66 [μm]. A failure boundary of 1.66 [μm] is chosen since this equals the accuracy requirement of 2 [μm] minus the measuring inaccuracy of 0.36 [μm], as discussed in Section 3.2.3. With this boundary of 1.66 [μm], it can be stated that these test results are below the lateral accuracy requirement. Out of the successful tests, this is only the case for gap height 125 [μm] test 2. Therefore out of the 19 valid shrinkage predictions, only one failed.

The 10th and 11th columns show the final accuracy results, the y- and x-coordinate respectively. These results show the positioning difference between the desired and final lens positions after the adhesive curing. Again the failure boundary of $\pm$ 1.66 [μm] is chosen for these results. As can be seen in the 10th column, three tests show a final lens y-shift above this boundary. Two of these failed tests are caused by exceeding the arc length requirements. For gap height 75 [μm] test 1, the shrinkage was under-predicted and the provided compensation was below the predicted lens shrinkage resulting in an accuracy failure. All the lens x-shifts were below the accuracy requirements, showing that the curing strategy was successful in minimizing the adhesive shrinkage-induced x-shift. The 12th column shows the square root of the x-and-y-displacement results. If this value is above 2.35 [μm] the accuracy requirements are not met and therefore indicated in red.

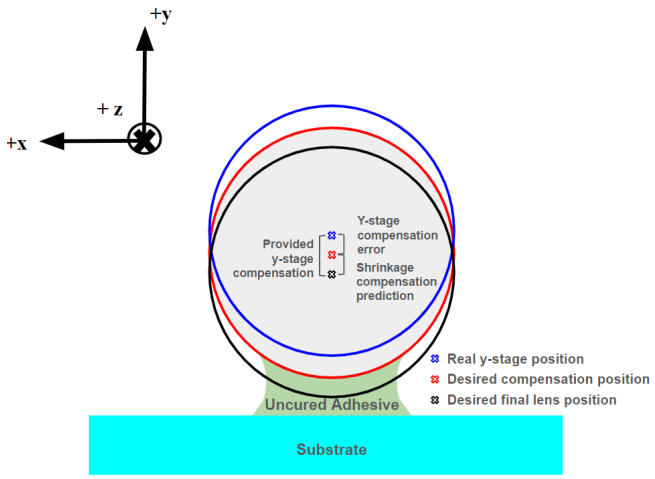

Figure 4.18: Exaggerated illustration indicating the: provided y-stage compensation, shrinkage compensation prediction, and y-stage compensation error.

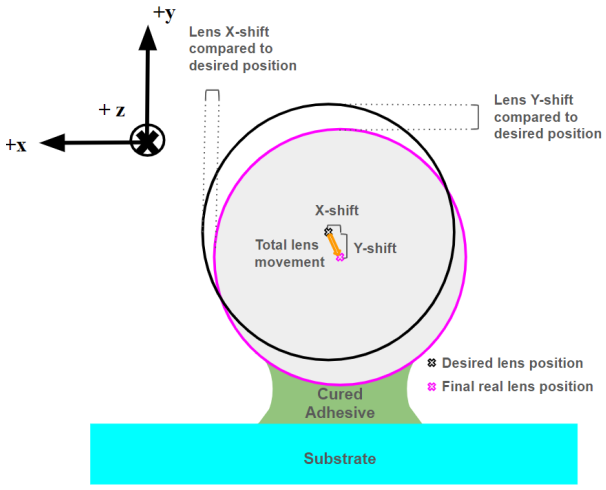

Figure 4.19: Exaggerated illustration indicating the lens x- and y-shift compared to the desired position, and the total lens movement.

Table 4.2: Overview of the V2 (orange test numbers and V3 (white test numbers) adhesive bond test strategy results, where the last four columns show the important final test results such as the shrinkage prediction error and the shrinkage induced lens shifts compared to the desired position.

50 [μm] tests	**Drop volume [μL]**	**Arc length [μm]**	**Shrinkage compensation prediction [μm]**	**Provided y-stage compensation [μm]**	**Y-stage compensation error [μm]**	**Shrinkage induced lens Y-shift [μm]**	**Linear Y-shrinkage relative to gap**	**Shrinkage prediction error [μm]**	**Lens Y-shift compared to desired position [μm]**	**Lens X-shift compared to desired position [μm]**	**Total lens movement compared to desired position [μm]**
1	1,51	0,88	5,95	7,24	-1,30	6,35	12,70%	0,40	0,55	0,65	0,85
2	0,60	0,84	5,94	5,80	0,13	4,51	9,01%	-1,43	1,29	1,22	1,78
3	0,29	0,75	5,34	4,47	-0,86	4,05	8,11%	-1,28	0,42	0,04	0,42
75 [μm] tests											
1	0,84	0,88	5,41	4,12	1,29	6,54	8,73%	1,14	-2,43	-0,05	2,43
2	1,05	0,81	5,41	4,14	1,27	4,72	6,29%	-0,70	0,63	0,23	0,67
3	0,93	0,70	5,29	4,75	-0,54	4,88	6,51%	-0,41	-0,13	0,61	0,63
100 [μm] tests											
1	1,74	0,77	6,31	6,50	-0,19	4,58	4,58%	-0,68	1,50	-0,55	1,60
2	0,65	0,65	5,26	6,98	1,71	5,57	5,57%	0,31	1,41	-0,14	1,41
3	1,66	0,74	5,26	4,16	-1,10	5,72	5,72%	0,46	-1,56	0,04	1,56
125 [μm] tests											
1	1,08	0,83	5,09	6,15	-1,06	6,18	4,94%	1,09	-0,03	-0,01	0,03
2	1,36	0,76	5,27	5,75	-0,48	7,23	5,79%	1,97	-1,49	1,33	1,99
3	1,26	0,84	5,24	4,34	-0,89	5,29	4,24%	0,05	-0,95	0,94	1,33
150 [μm] tests											
1	2,25	1,01	5,22	4,68	-0,54	7,13	4,75%	1,91	-2,45	-0,15	2,45
2	0,97	0,88	5,22	6,91	1,69	6,51	4,34%	1,29	0,40	-1,19	1,25
3	1,45	0,93	5,22	5,23	0,01	5,59	3,73%	0,37	-0,36	0,11	0,37
175 [μm] tests											
1	0,45	0,76	5,00	5,44	-0,44	5,81	3,32%	0,81	-0,37	0,53	0,64
2	0,69	0,70	5,03	4,47	0,56	3,89	2,22%	-1,14	0,58	0,58	0,82
3	0,34	0,56	5,20	3,63	-1,57	0,06	0,04%	-5,14	3,57	1,69	3,95
200 [μm] tests											
1	0,79	0,76	4,95	6,03	-1,08	4,58	2,29%	-0,37	1,44	1,01	1,77
2	0,37	0,63	4,97	5,33	-0,36	3,87	1,94%	-1,10	1,46	0,32	1,49
3	0,78	0,73	5,19	4,41	-0,78	3,91	1,96%	-1,28	0,50	1,21	1,31

4.9.2. Repeatability

The average results and standard deviations of the test strategy outcomes, including the final lens y- and x-shift, the square root of these shifts, and the final shrinkage prediction errors, are derived from the prediction model V3 data in Table 4.2, and presented in Table 4.3. These strategy outcomes are illustrated in Figure 4.19. It can be seen that all the averages, besides the total lens movements, show sub-micrometer precision. The results from Table 4.3 show that:

- The final lens y-shift has a sub-micrometer repeatability of $\pm$ 0.93 [μm].
- The final lens x-shift has a sub-micrometer repeatability of $\pm$ 0.74 [μm].
- The total lens movement compared to its desired position has a sub-micrometer repeatability of $\pm$ 0.48 [μm].
- The shrinkage prediction error has a sub-micrometer repeatability of $\pm$ 0.89 [μm].

Considering these averages and standard deviations for the final accuracy results, it can be concluded that the accuracy requirements are met by implementing this adhesive bonding test strategy.

Table 4.3: Overview of test strategy averages and repeatability results, considering lens x- and y-shifts, total lens movement, and shrinkage prediction errors.

	Lens Y shift compared to desired position [μm]	**Lens X shift compared to desired position [μm]**	**Total lens movement [μm]**	**Shrinkage prediction error [μm]**
Average	-0,03	0,20	1,04	-0,06
Standard deviation	0,93	0,74	0,48	0,89

4.9.3. Shrinkage induced lens rotation results

Rotations around the x-axis caused by the adhesive shrinkage are not allowed to exceed angle shifts above 0.23 [Deg] when the lens is aligned to the optical axis from the laser diode. The lens may be angled relative to the substrate if the optical axis is not parallel to it. Therefore, when positioning the lens at an angle relative to the substrate, the angle deviation around the x-axis must not exceed 0.23 degrees.

The bonding test strategy does not affect rotations around the y-axis. The liquid bridge formed between the lens and the substrate is symmetrical about the plane shown in Figure 4.20. However, the symmetry of the bond can be affected if a more viscous adhesive is used. This symmetry is maintained along the entire length of the adhesive bridge, as the lowest point of the lens is always centered within the liquid bridge. Since a symmetric bond along the line of the lowest point of the lens is formed, and since the adhesive is cured from below, it is assumed that no unwanted rotations occur around this plane. These rotations could not be measured, as capturing the necessary images would require viewing the lens from above or below. The current setup does not support this orientation for image capturing.

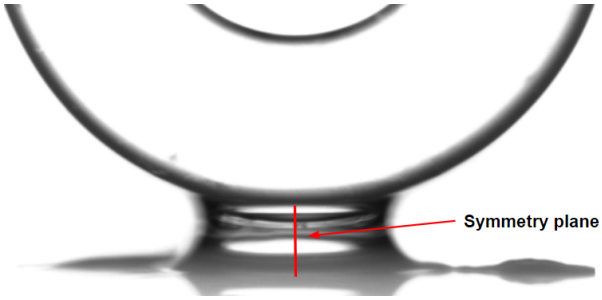

Figure 4.20: Front image of the bond and the symmetry plane around the middle of the lens.

The Rx rotation results have been extracted with the data from the ”side tests”. During these side tests, the CCD camera was in line with the x-axis, ensuring a proper side view of the lens, and substrate angle. Multiple images, like shown in Figure 4.21 have been made for the side tests for both the uncured and cured situations. Out of these images, information like the lens angle (angle between horizon and red line), substrate angle (angle between horizon and blue line), left gap height (LG, green line), and right gap height (RG, green line) have been extracted. This data is gathered and used to calculate the relevant data shown in Table 4.4.

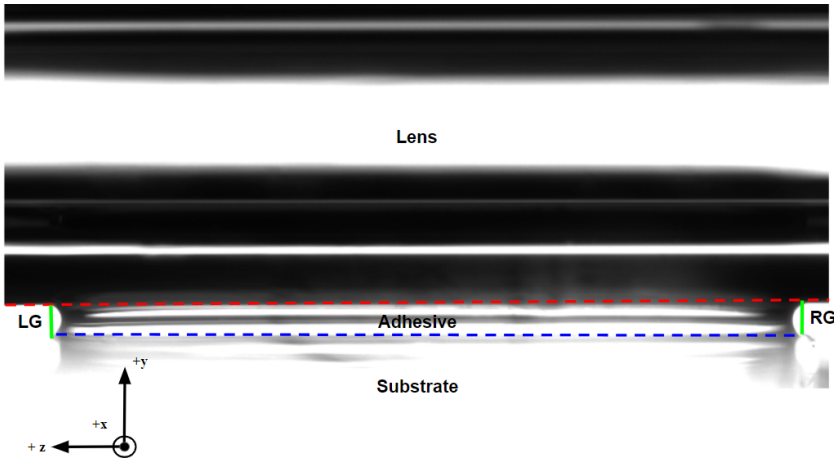

Figure 4.21: Side test image example showing the lens angle (between the horizon and the red dashed line) and the substrate angle (between the horizon and the blue dashed line).

The data shows that for small substrate-lens angles, there exists no measurable angle change between the substrate and the lens. This can be attributed to the slight angle difference between the lens and the substrate, along with the adhesive's low shrinkage. The gap height difference between the LG and RG is minimal. In the most extreme case during these tests, a 0.27-degree difference results in a shrinkage difference of only around 0.71 [μm] between both sides.

Table 4.4: Angle change around the x-axis measurements and results.

Test number	**Gap height pre-curing [μm]**	**Linear Y shrinkage relative to gap**	**Substrate-lens angle difference pre-curing [Deg]**	**Substrate-lens angle difference post-curing [Deg]**
1	52	10,02%	0,02	0,02
2	97	5,19%	0,04	0,04
3	171	3,17%	0,09	0,09
4	230	2,35%	0,08	0,08
5	172	3,33%	0,27	0,27

In conclusion, a small angle between the lens and the substrate does not result in a measurable or performance-impacting angle change. When looking at the accuracy requirements in Table 4.5 an allowable rotation around the optical axis of 0.23 [deg] is allowed within the active alignment step of the endoscopic probe assembly. If this is achieved within the active alignment, the bonding part of the assembly does not increase this lens rotation. In test 5, a substrate-lens angle difference of 0.27 [deg] was measured. The results from this test show that the angle stays the same, making it a proper strategy to keep the lens rotations within the prescribed target to align the lens with the optical axis. By implementing the adhesive bonding strategy, the lens will not rotate outside the rotation requirements of 0.23 [Deg] if the optical axis is not perfectly parallel with the substrate.

Table 4.5: Adhesive bonding test strategy lens rotation results and repeatabilities.

	Goal	Angle change results	Repeatability
Rx	<0.23 ∘	0.00 ∘	0.00 ∘
Ry	<0.23 ∘	0.00 ∘	0.00 ∘

4.10. Bond strength results

In addition to the precise bonding of the lens, an important factor is the bond strength that secures the connected parts. Since the endoscopic probes need to get miniaturized, the components get smaller and the volume of adhesive used is also likely to get down. This would result in a smaller bond area, lowering the bonding strength. For these reasons, tensile strength tests will have to be conducted to ensure a strong and reliable bond for the fragile components.

A bond strength setup was designed and manufactured to test the bond strength, shown in Figures 4.22 and 4.23. This setup had been designed to connect the lens to the main station, indicated with ”1” in Figure 4.22. The lens-substrate bond (2) can firmly be inserted into this main station using a form-fit connection. Then the stress platform (3) is positioned on top of the substrate that is bonded with the lens. A force is incrementally applied to the stress platform by adding mass, in steps of 10 grams near the failure point, until the bond fails, as shown in Figure 4.23.

Before conducting these tests, each bond must be carefully inspected beneath the CCD sensor to determine both the adhesive-lens contact area and the adhesive substrate contact area. With this data, the expected bond strength can be calculated as well as the actual bond strength per square millimeter. For these bond strength tests, there is only looked at the tensile strength.

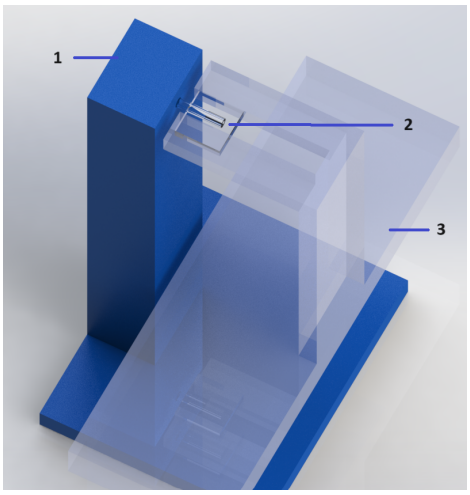

Figure 4.22: The adhesive bond strength test setup: (1) Main station; (2) Lens-substrate bond; (3) Stress platform.

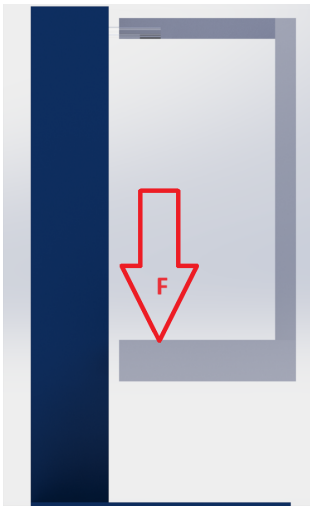

Figure 4.23: Side view of the adhesive bond strength test setup, with the red F-arrow indicating the direction of force applied to the stress platform and subsequently to the bond.

4.10.1. Inadequate surface cleaning

To test the importance of the cleanliness of the surfaces on the bond strength, the lens has not been cleaned for a few test samples. Upon examining the post-tensile failure bond, it is evident that the failure occurs at the adhesive-lens interface, shown in Figure 4.24 where there is a clean separation between the lens and the cured adhesive. This observation is logical because the adhesive-lens interface, representing the smallest adhesive-part area, has the most significant impact on the overall bond strength.

Figure 4.24: Front view of bond failure, showing the lens surface untreated with isopropanol. The image highlights a clean separation between the lens and the adhesive.

The results of eight inadequate surface cleaning bond tests are shown in Table 4.6. The results showed that an average tensile bond strength of 1.07 [MPa] can be achieved, equal to 1.07 [N/mm^2]. This is almost a factor of 10 smaller than the bond strength shown in the technical data sheet of the Uvacryl 2661 adhesive, which promises an adhesion to glasses of 9.7 [MPa]. These results highlight the importance of thoroughly cleaning the lens and substrate surfaces to achieve optimal bond strength.

Table 4.6: Inadequate lens cleaning bond strength test results.

Test number	Gap height [μm]	Adhesive-lens contact area [mm^2]	Applied tensile force failure [N]	Adhesive tensile Strength [MPa]
1	50	5,09	5,37	1,06
2	50	5,08	5,35	1,05
3	100	4,42	4,76	1,08
4	100	4,21	4,17	0,99
5	150	3,32	3,38	1,02
6	150	2,97	2,99	1,01
7	200	2,30	2,70	1,17
8	200	2,07	2,50	1,21

4.10.2. Adequate surface cleaning

The results from the bond strength tests that have been conducted can be seen in Table 4.7. With an average tensile bond strength of 4.10 [MPa], it shows that the tensile bond strength is 4 times stronger compared to the inadequate surface cleaning tests. The final obtained adhesive tensile strength is still half of the promised strength, this is likely caused by the implemented curing parameters, that differ from the parameters used by the manufacturer. It should be noted that when increasing the gap the tensile failure force decreases since the adhesive-lens contact area decreases, therefore, an excessively large gap height is not recommended, as it reduces the overall force the bond can withstand before tensile failure.

Table 4.7: Adequate lens cleaning bond strength test results.

Test number	Gap height [μm]	Adhesive-lens contact area [mm^2]	Applied tensile force failure [N]	Adhesive tensile Strength [MPa]
1	50	3,25	14,27	4,39
2	50	2,55	11,08	4,35
3	100	2,85	12,38	4,35
4	100	2,04	9,19	4,50
5	150	1,97	7,69	3,90
6	150	2,42	9,19	3,79
7	200	1,75	7,03	4,03
8	200	1,72	6,04	3,52

Examining Figures 4.25, 4.26, and 4.27, it can be seen that the post-tensile failure bond is more disrupted compared to the post-failure bond from Figure 4.24. This is attributed to improved adhesion to the cleaned lens surface, resulting in adhesive residue remaining on the lens after tensile failure, as shown in Figure 4.27.

Figure 4.25: Side view of post-failure bond that is connected to the substrate.

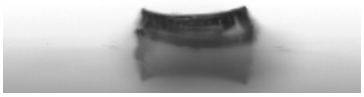

Figure 4.26: Front view of post-failure bond that is connected to the substrate.

Figure 4.27: Side view of post-failure bond that is connected to the lens.

5

Adhesive Bonding Strategy

The adhesive bonding test strategy as discussed in Chapter 4, is redesigned for application, allowing it to be implemented in future assembly processes without the need for the same setup, materials, and parts. An overview and explanation of the adhesive bonding strategy will be provided after which important strategy preparations will be elaborated. This chapter concludes with an overview of important operational requirements for the adhesive bond strategy. This chapter can be seen as the instruction manual encompassing all the relevant aspects covered in Chapter 3 and 4.

5.1. The adhesive bonding strategy

The strategy starts by cleaning the surfaces of both the substrate and the to-be-bonded optical components. Isopropanol is recommended as a cleaning agent; however, it is essential to verify its approval in the adhesive's technical data sheet. This step is followed by the optical alignment procedure, in which the desired coordinates of the optical component are determined. Once the desired coordinates are established, the gap height between the component and the substrate must be measured and inputted in the constructed shrinkage prediction model.

The optical part must be removed from its desired position above the substrate, such that a precisely controlled volume of adhesive can be dispensed onto the substrate. To minimize the risk of creating an asymmetrical bond geometry that could lead to unwanted shrinkage-induced component shifts, it is advisable to dispense the adhesive drop precisely at the position where the center of the optical component will be placed. This precise droplet positioning is particularly essential if a viscous adhesive is used. After the drop is dispensed the optical component can be positioned back to the desired position. For this position, a liquid bridge should be formed between the substrate and the optical component.

The shrinkage prediction model, as detailed in Section 5.2, is an algorithm that is designed to estimate the compensation required for positioning the optical component accurately after adhesive curing. The calculated y-compensation must be applied to the optical component, followed by curing the adhesive under the curing conditions as outlined in the strategy preparations. When the required UV dose is applied to fully cure the adhesive, the optical component is precisely bonded to the substrate, achieving an alignment accuracy within the target precision.

The adhesive bonding strategy and essential preparatory steps are schematically illustrated in Figure 5.1. The preparatory steps are highlighted in the red box. The bonding strategy is outlined in the blue box. To successfully implement this strategy in micro-optical component assembly, all steps must be followed accordingly. Numbers are assigned to specific steps in the strategy to indicate when images should be taken for process verification and data extraction. The explanation for each numbered step is provided on the left side of Figure 5.1.

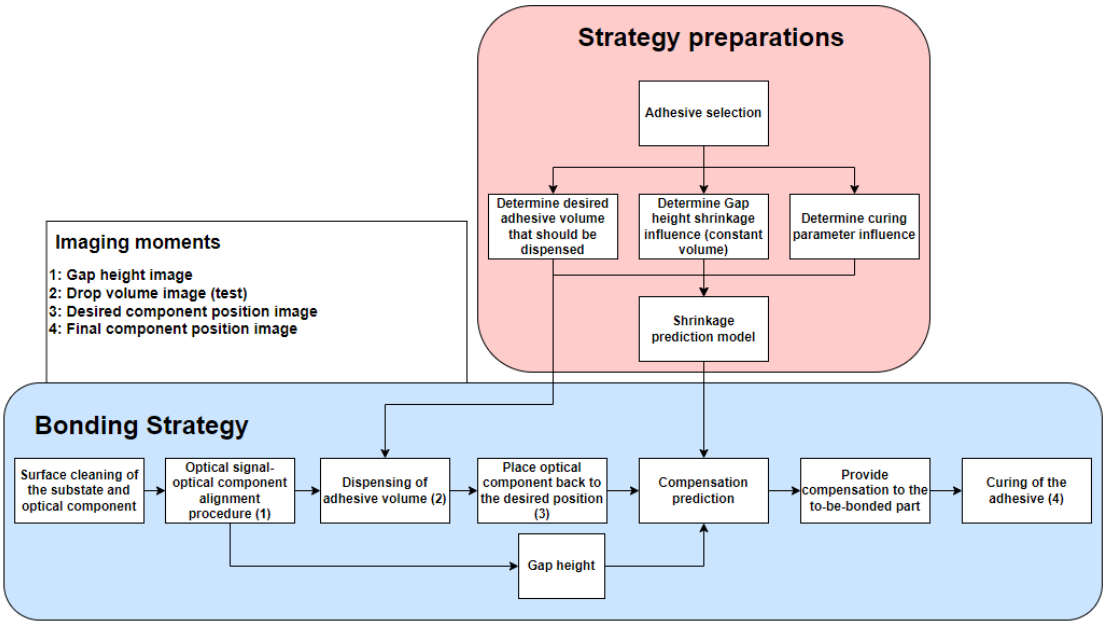

Figure 5.1: Adhesive bonding strategy block diagram, with numbers in the blocks corresponding to the image moments explained on the left.

5.2. Strategy preparations

Before implementing the bonding strategy, four preparatory steps must be completed. These steps involve constructing the shrinkage prediction model. The preparatory steps are discussed in detail below.

The four essential steps required to construct the shrinkage prediction model are as follows:

1. Selecting an appropriate UV adhesive.
2. Assessing the curing parameter influences on adhesive shrinkage.
3. Determine the desired adhesive volume that should be dispensed.
4. Determining the relationship between gap height and the linear shrinkage-induced component y-shift for a constant adhesive volume.

These relationships and influences can be quantified by collecting shrinkage-induced component displacement data.

This strategy is designed for UV-curable adhesives. The initial preparatory step involves selecting the adhesive. Key performance considerations, such as viscosity, shrinkage, and adhesion to the required materials, must be identified and rated on importance. These considerations should be evaluated based on the specific use case for the bonding strategy. Evaluate these performance considerations for a selection of adhesives and choose the one that best aligns with the desired performance criteria.

When the adhesive is selected, tests need to be conducted on the curing parameter influences on the adhesive shrinkage. As discussed in Section 3.3.1, curing parameters such as UV intensity, curing duration, and the UV-laser spot-adhesive distance should be taken into account and tested since they influence the final adhesive shrinkage. Check the technical data sheet for the required UV dose to fully cure the adhesive. Choose the curing parameters that give the lowest amount of shrinkage while still providing sufficient bonding to the parts. Reducing the adhesive curing time to a minimum value is not desirable since this can cause poor adhesive performance depending on the adhesive used. The substrate/housing should be designed to facilitate curing from beneath the substrate, thereby minimizing horizontal shifts induced by adhesive shrinkage on the optical components.

To determine the appropriate adhesive volume for dispensing, consider the largest gap height and the minimum desired bond strength. The adhesive volume should be such that the required bond strength is met for the largest gap height. The largest gap height is critical as it represents the scenario with the lowest bond strength due to minimal adhesive-lens surface area. Dispensing a larger volume improves contact areas between the adhesive, substrate, and optical components, enhancing bonding strength. Consistently dispensing this volume across all gap heights ensures optimal shrinkage prediction and mitigates volume-induced displacements of the lens caused by shrinkage.

Once the required curing parameters and desired adhesive volume are set, gap height tests should be conducted. Define the gap height boundaries. Test the shrinkage for varying gap heights, using the predetermined adhesive volume. Measure the shrinkage-induced optical component y-shifts and construct a best-fit line from the data points. This line predicts the shrinkage based on a gap height that should incorporated into the prediction model. Start at the smallest gap height, and use a convenient step size up to the largest gap height, performing a minimum of two tests per gap height.

A block scheme of the shrinkage prediction model is shown in Figure 5.2. When entering the curing parameters and gap height the vertical component compensation can be calculated by the shrinkage prediction model. Setting up this model mathematically involves conducting adhesive experiments, measuring shrinkage at different gaps, and fitting the curve as discussed in Section 3.4. Based on the gap height the calculated compensation should be added to the optical-component alignment coordinates before curing the adhesive.

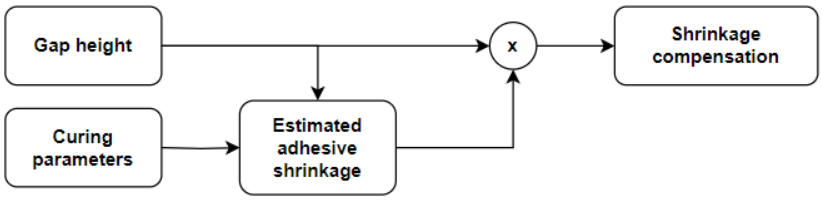

Figure 5.2: Shrinkage prediction model block scheme.

5.3. Operating requirements for shrinkage compensation bonding strategy

The designed shrinkage compensation strategy works within specific operating requirements: gap height requirements, setup requirements, and procedure requirements. These requirements must be met to achieve lens shrinkage compensation within the accuracy demands specified in Section 2.1.

5.3.1. Gap height requirements

The gap height needs to be within specific bounds to position the lens accurately and properly with this adhesive bonding strategy. This bound was tested by lowering the gap height from 100 [μm] with steps of 25 [μm]. The minimum gap height for this compensation test strategy was found to be 50 [μm]. If the gap height is below this distance inaccurate compensation is calculated by the shrinkage prediction test model. This could be caused by inadequate model calibration. The prediction model is not accurately calibrated for gap heights below 50 [μm] since most tests were done between 50 and 200 [μm].

From a gap height of 25 [μm] and below the shrinkage prediction test model calculates a compensation that exceeds the actual shrinkage induced y shift, resulting in a bonding accuracy exceeding 2 [μm]. Therefore, if the desired gap height is below 50 [μm], an additional shrinkage prediction calculator should be constructed. This extra model predicts the shrinkage-induced displacements between gap heights between 1 and 50 [μm] which differs from the shrinkage prediction model for gap heights between 50 and 200 [μm].

The maximum gap height is determined by the minimum allowable adhesive-lens contact area. Within the bonding test strategy tests, a gap height above 200 [μm] resulted in an adhesive-lens contact area below 1.5 [mm^2], resulting in a shrinkage force that is too low to bend the cantilever beam used in the test setup. This maximum gap height is therefore determined by the cantilever beam design. Take into account that for increasing gap height the bond strength becomes weaker since the adhesive-optical component contact area decreases considering a consistent adhesive volume. In the case study of the GRIN-lens assembly for miniaturized endoscopic probes, it is essential to minimize the gap height to reduce the diameter of the probe head. This reduction enhances the probe's accessibility, enabling it to reach into small veins and other confined anatomical structures. Considering the endoscopic probe design by Li et al. [23], with a probe diameter of 0.69 µm, a gap height of 200 µm would account for 29% of the total probe diameter, which is a significant fraction in terms of packaging efficiency.

5.3.2. Setup requirements

To achieve precise optical component bonding, the setup must meet specific requirements. The four most critical requirements for the setup are:

- **Y-stage accuracy requirements:** The y-stage used for the bonding strategy requires positioning accuracy below the accuracy requirements minus the shrinkage prediction error standard deviation. Achieving a better accuracy is preferable due to the inherent inaccuracies in the shrinkage prediction. As such, when the y-stage positioning accuracy approaches the accuracy set in the requirements, more tests are likely to fall outside the required accuracy range, thereby reducing the strategy's repeatability.

- **Optical component and substrate fixation requirements:** The fixation of the optical component and substrate needs to be stronger than the shrinkage forces that will act on it. If this is not the case, the optical component and/or substrate will move and rotate when curing the adhesive. This would reduce the reliability and accuracy of the bonding strategy.

- **CCD camera/lens requirement:** The combination of the CCD camera and the telecentric lens used, provided a pixel size of 1.725 [μm] after calibration. This pixel size provides a measuring deviation of $\pm$ 0.36 [μm], 20.87% of the pixel size. A maximum measurement error of 0.50 [μm] would be sufficient to maintain the reliability of the measurements and strategy results, as 85% of the shrinkage prediction errors from the conducted tests are below 1.50 [μm]. Therefore the pixel size should be at least below 2.396 [μm].

- **Cantilever beam requirements:** The cantilever beam that positions the to-be-bonded object needs to have a stiffness such that it bends under the shrinkage forces that are acting on the to-be-bonded object. However, the stiffness should be higher than the viscosity forces that are introduced when lowering or lifting the object to get the desired gap height.

5.3.3. Procedure requirements

The procedure also needs to meet specific requirements. This category of requirements concerns material usage and handling. The six requirements are:

- **Surface cleaning requirements:** Both parts that need to be bonded together should be carefully cleaned to remove grease and other small particles that influence the surface wetting and the bond strength. Within this research, all parts have been cleaned with isopropanol.

- **Shape of the to-be-bonded parts:** Within this research a cylindrical lens is bonded to a flat substrate. The shapes of these parts influence the bond geometry and therefore change the adhesive shrinkage behavior. If other shapes need to be bonded accurately, the shrinkage behavior should be tested, and the results should be incorporated into the shrinkage prediction model. A circular bottom surface for the to-be bonded component is recommended, as it helps center the adhesive drop in the desired position.

- **Adhesive requirements:** This research is only based on the adhesive behavior of the Viba Uvacryl 2751 glue. Significant shrinkage variations exist between different adhesives. If a different adhesive needs to be used, the shrinkage behavior across varying gap heights and dispensed

adhesive volumes should be tested and incorporated into the shrinkage prediction model. Fresh Uvacryl 2751 adhesive is used for these tests and should be used to get similar results. If the same adhesive is used near its expiration date or after it has expired, a significant increase in the shrinkage standard deviation can be observed. This shrinkage behavior would likely lead to poorer positioning results [24].

- **Dispensing requirements:** The dispensing method should be capable of delivering drops with an accuracy of 0.1 [μL]. See Appendix E for additional elaboration about this dispensing accuracy requirement. This requirement contributes to a more accurate shrinkage prediction. Dispensing methods like jet dispensing [25] or ultra-micro pin dispensing [26] could be integrated into the strategy procedure.
- **Lens-substrate x-positioning:** To ensure that the majority of the adhesive drop forms the liquid bridge, the center of the component must be aligned above the center of the adhesive drop. If this alignment is not achieved, part of the adhesive will not contribute to forming the liquid bridge between the substrate and the component to be bonded. This issue is shown in Figure 5.3, where a significant portion of the adhesive drop is not utilized in forming the liquid bridge. Proper alignment of the lens center with the adhesive drop center ensures that the dispensed adhesive volume forms a complete liquid bridge, as shown in Figure 5.4. This alignment guarantees that the volume parameter, which influences the shrinkage prediction, accurately reflects the real scenario.

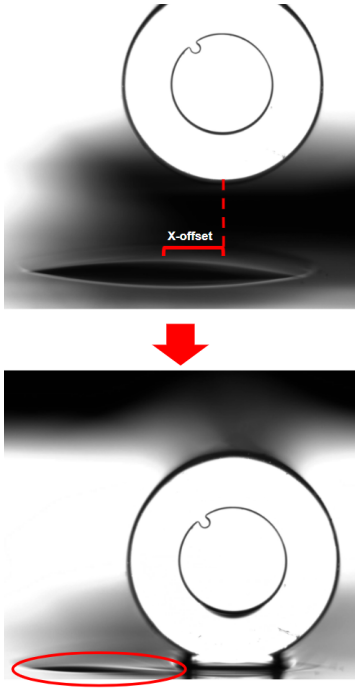

Figure 5.3: Example of bond-forming where a significant volume of the adhesive drop is not part of the liquid bridge between the substrate and the lens.

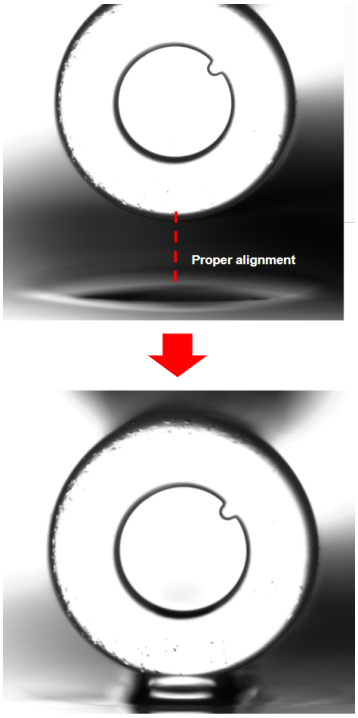

Figure 5.4: Example of bond-forming when the center of the adhesive drop is aligned with the center of the lens. The majority of the drop is used to form the bond.

- **Curing requirements:** The adhesive should be cured from below the substrate. This minimizes horizontal adhesive shrinkage-induced component shifts.

By taking these operating requirements carefully into consideration, the bonding strategy can be implemented into the assembly process of micro-optical devices, ensuring accurate and reliable positioning and bonding of optical components.

6

Discussion

The results from Chapter 4 indicate that the proposed adhesive bonding strategy of Chapter 5 is promising. This strategy has revealed principles, relationships, and generalizations essential for achieving accurate bonding of optical components using UV-curable adhesives. The first key findings consider relevant performance considerations that influence adhesive selection, such as shrinkage, viscosity, cure type, and adhesion to the desired materials. These adhesive properties should be carefully analyzed when selecting the adhesive.

Additionally, this study reveals how curing intensity variations and therefore variations in curing speed lead to varying degrees of volumetric and linear shrinkage. This shrinkage behavior was also observed in the research conducted by Hudson et al. [20]. Increased curing speed accelerates the polymerization reaction due to higher UV intensity, reducing the time available for adhesive molecules to rearrange. Consequently, this results in decreased volumetric and linear adhesive shrinkage. Limiting the linear adhesive shrinkage is preferred when aiming to accurately align optical components, so therefore a high curing intensity was chosen. This ensures more predictable and controlled changes in adhesive dimensions during curing. However, reducing the curing time to a minimum value is not desirable since extremely fast reactions can cause poorer adhesive bonding performance. The high curing rate used in this research likely contributed to the bond strength being lower than the specified bond strength.

Additionally, the orientation of the curing direction significantly impacts the optical component's x-shift magnitude. Curing from beneath the adhesive drop ensures uniform illumination of the bond, preventing tilts caused by uneven curing along the bond profile and thereby reducing x-shifts in optical components due to adhesive shrinkage. This curing direction behavior is in line with: the conclusions drawn from the literature research [14], and the research conducted by van Gastel et al. [27].

Moreover, variations in the gap height impact the linear shrinkage-induced lens displacement along the y-axis. For an increasing height between the substrate and the optical component, less total adhesive shrinkage-induced lens y-shift was measured. This was contrary to the intuitive expectation that adhesive shrinkage would be uniform across all dimensions, regardless of the gap height. This would lead to an assumption that greater gaps would result in more shrinkage. However, the change in shrinkage behavior is primarily influenced by the geometry of the adhesive bond, which is affected by the gap height. For a larger gap, the bond is taller, and the initial shrinkage of the adhesive tends to pull the uncured liquid adhesive downward before pulling down the lens. In contrast, for a smaller gap, the bond is shorter, and the contraction of the uncured adhesive has a more pronounced effect on the lens alignment. This is because the adhesive is more confined around the bottom of the lens, leading to a greater contraction of the lens. The confined space in a smaller gap height restricts the adhesive's ability to redistribute itself during curing, resulting in more significant shrinkage effects on the lens positioning. This adhesive behavior during curing should be validated in future work, through the implementation of a high-speed camera capable of capturing the dynamic changes in the adhesive's geometry throughout the curing process.

It was also observed that the dispensed adhesive volume directly influences the linear displacement of the optical component along the y-axis due to shrinkage. This shrinkage behavior is again influenced by changes in bond geometry resulting from variations in the dispensed adhesive volume. These findings highlight the critical role of controlling adhesive volume to mitigate shrinkage-induced displacements. This research faced challenges with volume control, leading to inconsistent shrinkage results across tests with fluctuating adhesive volumes. The volume influence on the shrinkage was not observed for the drop tests discussed in Section 3.3.1. Therefore, it can be concluded that the volume of the adhesive influences shrinkage when bonding parts together due to the adhesive geometry of the bond.

These observations yielded valuable insights into the shrinkage behavior within the specifically designed test setup employed for experimentation. The extracted shrinkage behavior and preferred process parameters resulted in the design of an adhesive bonding test strategy. This test strategy incorporates a shrinkage prediction algorithm that estimates the linear shrinkage-induced component shift percentage based on changes in the adhesive gap height. This test strategy is only valid within a certain dispensed adhesive drop volume range.

The shrinkage prediction test model proved to accurately predict the shrinkage-induced lens y-shift. Where the least accurate prediction resulted in a prediction error of 1.28 [μm] and the most accurate prediction had a prediction error of 0.04 [μm]. This deviation is likely caused by deviations in the dispensed volume and the adhesive shrinkage. The shrinkage prediction model resulted in a sub-micrometer repeatability of $\pm$ 0.89 [μm]. The results of the adhesive bonding test strategy proved that the lens can be positioned below the lateral accuracy requirements of 2 [μm]. The test results also showed sub-micrometer repeatability in both the x- and y-positioning of the lens. The difference between the shrinkage prediction and the final lens positioning accuracy is caused by the repeatability of the Y-stage that positions the lens and provides the shrinkage compensation. Since the adhesive is cured from below no x-compensation has to be provided to the optical component to keep the x-positioning accuracy below the target precision. The bonding strategy does not influence the rotation of the lens around the x-axis for substrate-lens angles below 0.27 [Deg].

It is important to note that variations in adhesive selection, component shapes, component materials, curing methods, and curing speed influence shrinkage behavior. By systematically testing and analyzing shrinkage behavior under controlled process parameters, a shrinkage prediction model can be developed to accurately align with the specific adhesive shrinkage characteristics and behavior. This shrinkage prediction model can then be implemented for the final adhesive bonding strategy, as discussed in Chapter 5. If more stringent precision targets are required, the setup should be capable of sub-micrometer positioning such that a shrinkage prediction can be accurately applied to the optical component. Additionally, the camera's pixel size, which measures displacements and adhesive behavior, should be reduced to enhance measurement precision. However, variations in adhesive shrinkage will inevitably occur from sample to sample due to changes in the degree of polymerization (number of covalent bonds formed) [16]. This inherent variability makes it challenging to precisely predict shrinkage for each bonding step.

Limitations regarding this research include the unilateral observation of shrinkage behavior, which restricted simultaneous viewing of both the front and side of the lens. This setup introduces potential observational biases, as the view from one angle may not fully represent the real-life shrinkage behavior occurring on all sides of the lens. Addressing this limitation would involve enhancing the setup with an additional camera capable of side-view imaging, necessitating adjustments to enable concurrent side-view observation and proper side illumination for imaging clarity. Another limitation involved the method of disconnecting the lens, which required significant force and occasionally caused small displacements of the lens after accurately bonding the lens to its desired position. This could be improved by considering alternative component-cantilever beam fixation methods, such as a vacuum gripper.

7

Conclusion

The results underscore the promising adhesive bonding strategy proposed in Chapter 5. The developed shrinkage prediction model ensures an accuracy below the target precision, enhancing optical component alignment and fixation. Overall, this study offers practical tools to optimize bonding processes, crucial for improving optical system reliability and performance in diverse applications.

This study contributed to five main findings that should be considered when implementing the adhesive bonding strategy into the micro-assembly process of optical components. These findings are:

1. The UV intensity of the curing process significantly impacts the adhesive's total volumetric and linear shrinkage. Higher UV intensity results in reduced adhesive shrinkage. This curing influence should be considered when collecting shrinkage data for constructing the shrinkage prediction model.
2. Curing the adhesive from below the substrate ensures uniform illumination of the bond, thereby minimizing shrinkage-induced x-shifts of the optical component. Consequently, a transparent substrate or housing is recommended. This approach eliminates the need for x-compensations.
3. As the gap between the substrate and the optical component increases for a constant adhesive drop volume, the linear shrinkage-induced lens y-displacement decreases. This height influence should be considered when developing the shrinkage prediction model.
4. As the adhesive volume increases, considering a consistent gap height, the shrinkage-induced y-shift of the component also increases. Consequently, an accurate dispensing method is necessary to ensure the dispensing of precise adhesive drop volumes. This will enhance the accuracy of shrinkage predictions.
5. The shrinkage prediction model should be developed by testing relevant process parameters that influence the adhesive shrinkage behavior. Properly addressing these factors enables the model to predict shrinkage-induced component y-shifts with sub-micrometer accuracy.

These key findings contributed to the design of the bonding strategy, resulting in an average shrinkage prediction error of 0.03 [μm] and an average final lens precision of 1.04 [μm] for gap heights ranging from 50 to 200 [μm]. The highest lens precision, 0.37 [μm], was achieved with a gap height of 150 [μm].

Building on the promising findings of this study, several pathways for future research can be explored to refine and implement the adhesive bonding strategy. These proposals aim to address the important factors influencing adhesive shrinkage and component alignment.

1. **Multi angle observation:** To overcome the limitations of unilateral observation, future studies should focus on developing multi-angle observation systems that can capture the shrinkage behavior from multiple perspectives simultaneously. This could involve integrating additional cameras and illumination sources into the setup, allowing for a comprehensive analysis of shrinkage-induced displacements. Implementing high-resolution imaging and advanced image processing

algorithms would enable precise measurement of shrinkage effects, leading to more accurate prediction models and a better understanding of the underlying mechanics.

2. **Comprehensive testing of process parameters:** Expanding the scope of testing by including a wider range of process parameters can contribute to constructing more robust shrinkage prediction models. Future research should systematically explore the effects of various factors such as adhesive composition, environmental conditions such as temperature and humidity, different shaped optical components, and different substrate materials on shrinkage behavior. By developing comprehensive datasets under diverse conditions, it is possible to create more accurate prediction models that can be applied to a broader range of applications.

3. **Implementation and validation in real-world applications:** Finally, future research should focus on implementing and validating the proposed adhesive bonding strategy in real-world optical systems. This involves collaborating with industry partners to test the strategy in practical applications, such as in the manufacturing of lenses, sensors, micro-medical optical devices, and other optical components. By conducting field trials and gathering feedback from industrial applications, it is possible to refine the strategy further and demonstrate its efficacy in enhancing the precision and reliability of optical assemblies.

By addressing these research areas, future studies can significantly advance the understanding and application of UV-curable adhesives in optical component bonding. The insights gained will contribute to the development of more robust and reliable bonding strategies, ultimately improving the performance of optical systems across various industrial and scientific domains.

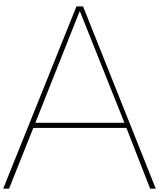

Cantilever beam Matlab code

Cantilever length calculations:

```
% Parameters
spring_constant_N_per_mm = 3; % N/mm  (flexible test beam)
youngs_modulus_Pa = 215000 %e11; % Pa
thickness_mm = 0.85; % mm
width_mm = 12.7; % mm

% Convert width to meters
width_m = width_mm / 1000; % convert mm to meters

% Calculate second moment of area (moment of inertia)
I_needed_mm4 = (1/12)*width_mm*(thickness_mm^3); % in mm^4
disp(['Needed second moment of area (I): ' num2str(I_needed_mm4) ' mm^4'])
    ;

% Calculate length of cantilever beam
length_needed_mm = (3 * I_needed_mm4 * youngs_modulus_Pa /
    spring_constant_N_per_mm)^(1/3); % in mm
disp(['Length of the cantilever beam: ' num2str(length_needed_mm) ' mm']);
```

Cantilever thickness calculations:

```
%calculate thickness based on spring constant, beam length and width
% Parameters
spring_constant_N_per_mm = 3; % 3N/um (flexible test beam)
youngs_modulus_Pa = 215000  %e11; % Pa  N/mm^2
length_mm = 51.8927; % mm
width_mm = 12.7; % mm

% Convert width to meters

%width_m = width_mm / 1000; % convert mm to meters

% Calculate second moment of area (moment of inertia)
I_needed_mm4 = (spring_constant_N_per_mm * ((length_mm)^3)) / (3 *
    youngs_modulus_Pa); % in mm^4
disp(['Needed second moment of area (I): ' num2str(I_needed_mm4) ' mm^4'])
    ;

% Calculate thickness of cantilever beam
```

```
thickness_needed_mm = (I_needed_mm4 * 12 / width_mm)^(1/3); % in mm
disp(['Thickness of the cantilever beam: ' num2str(thickness_needed_mm) '
    mm']);

%%

% Section break for calculating displacement under a given mass
disp('--------------------------------------');

% Given parameters for displacement calculation
mass_kg = 0.005; % kg
gravity_m_per_s2 = 9.81; % m/s^2

% Calculate force exerted by the mass
force_N = mass_kg * gravity_m_per_s2; % N
disp(['Force exerted by the mass: ' num2str(force_N) ' N']);

% Calculate displacement of the cantilever beam under the given mass
displacement_mm = (force_N * length_mm^3) / (3 * youngs_modulus_Pa *
    I_needed_mm4); % in mm
disp(['Displacement of the cantilever beam under the given mass: ' num2str
    (displacement_mm) ' mm']);
```

B

Curing influence data

Table B.1: Curing direction influence on shrinkage-induced x-shift if the lens.

Curing from below the substrate		**Curing from above the substrate**	
Gap height [μm]	**X-shift lens [μm]**	**Gap height [μm]**	**X-shift lens [μm]**
11	0,72	0	1,73
18	0,98	0	0,00
60	0,00	35	1,44
65	0,00	52	1,87
74	1,33	92	1,80
97	0,38	98	3,31
100	0,00	140	3,59
100	0,07		
101	0,11		

Table B.2: Curing speed influences for drop diameter, height, volume, and contact angle.

Test nummer	Cure parameters	Diameter shrinkage %	Angle reduction %	Height shrinkage %	Volumetric shrinkage %
1	60% 60 sec	-3,97%	-40,00%	-14,04%	-47,05%
2	60% 60 sec	-3,63%	-28,57%	-12,10%	-36,39%
3	60% 60 sec	-3,73%	-26,67%	-10,89%	-34,91%
4	60% 60 sec	-3,65%	-25,00%	-11,54%	-33,31%
5	60% 60 sec	-3,17%	-10,34%	-11,19%	-18,78%
6	60% 60 sec	-4,01%	-11,54%	-10,78%	-21,91%
7	60% 60 sec	-3,02%	-5,56%	-12,67%	-14,02%
8	75% 45 sec	-1,68%	-6,25%	-11,11%	-11,03%
9	75% 45 sec	-2,03%	-11,43%	-12,50%	-16,99%
10	75% 45 sec	-2,42%	-22,22%	-13,58%	-28,21%
11	75% 45 sec	-2,22%	-6,67%	-9,68%	-12,87%
12	75% 45 sec	-2,67%	0,00%	-9,02%	-7,81%
13	75% 45 sec	-2,56%	8,00%	-9,84%	0,06%
14	75% 45 sec	-2,53%	-3,03%	-9,38%	-10,29%
15	100% 24 sec	-3,38%	81,25%	-7,19%	68,59%
16	100% 24 sec	-1,78%	-13,16%	-8,73%	-18,08%
17	100% 24 sec	-1,96%	-12,50%	-7,09%	-17,80%
18	100% 24 sec	-2,53%	0,00%	-9,09%	-7,39%
19	100% 24 sec	-2,13%	0,00%	-6,21%	-6,26%
20	100% 24 sec	-2,53%	-1,23%	-6,00%	-8,57%
21	100% 24 sec	-3,13%	-17,65%	-6,25%	-25,50%
22	100% 24 sec	-2,31%	-7,14%	-6,27%	-13,56%
23	100% 24 sec	-2,88%	-5,88%	-10,48%	-13,94%
24	100% 24 sec	-2,29%	-9,09%	-12,40%	-15,40%

C

Adhesive Bond geometry data

Table C.1: Contact angle adhesive-substrate and contact angle adhesive-lens data.

Test nummer	**Contact angle substrate [Deg]**	**Contact angle lens [Deg]**
1	10	21
2	14	22
3	15	19
4	16	19
5	14,5	18,5
6	13	20
7	18	19,5
8	16	20,5
9	17,5	20
10	18	20,5
Average	**15,2**	**20**

Table C.2: Gap height, shrinkage-induced lens shift data for tests with an adhesive drop volume between 0.3 and 0.7 [μL].

Adh volume [μL]	**Gap height [μm]**	**Lens Y-shift [μm]**	**Y shrinkage %**	**Lens X-shift [μm]**
0,7	50	4,67	9,34%	0,17
0,3	50	4,33	8,67%	0,04
0,6	50	4,51	9,01%	1,22
0,6	60	6,01	10,02%	0,11
0,7	69	6,40	9,28%	-0,05
0,3	75	4,54	6,06%	0,07
0,4	80	4,83	6,03%	0,72
0,6	100	4,58	4,58%	-0,55
0,4	100	5,12	5,12%	0,07
0,4	100	4,96	4,96%	0,05
0,4	100	3,83	3,83%	0,70
0,7	150	6,63	4,42%	0,01
0,4	175	5,81	3,32%	0,53
0,7	175	3,89	2,22%	0,52
0,4	200	3,87	1,94%	0,32

Table C.3: Measured data for the volume/arc length influence on the shrinkage induced lens y-shift.

Gap Height [μm]	**Drop volume [μL]**	**Arc length [mm]**	**Lens Y-shift**
50	0,70	0,86	9,34%
50	0,29	0,75	8,11%
50	1,51	0,88	12,70%
50	0,60	0,84	9,01%
75	0,84	0,88	8,73%
75	1,05	0,81	6,29%
75	0,93	0,70	6,51%
100	1,74	0,77	4,58%
100	0,65	0,65	5,57%
100	1,66	0,74	5,72%
125	1,08	0,83	4,94%
125	1,36	0,76	5,79%
125	1,26	0,84	4,24%
150	2,25	1,01	4,75%
150	0,97	0,88	4,34%
150	1,45	0,93	3,73%
175	0,45	0,76	3,32%
175	0,69	0,70	2,22%
175	0,34	0,56	0,04%
200	0,79	0,76	2,29%
200	0,37	0,63	1,94%
200	0,78	0,73	1,96%

D

Bonding strategy data

Table D.1: Dispensed volume data, calculated using the drop-shape analysis based on the contact angle and the drop diameter.

Contact angle [Deg]	Diameter [μm]	Drop volume [μL]
16	3788	1,51
17,4	2700	0,60
16	3120	0,84
16	3357	1,05
10	3774	0,93
16	3384	1,08
14	3828	1,36
18	3428	1,26
17	2470	0,45
14	3050	0,69
7	3042	0,34
15	3120	0,79
17,5	2295	0,37
14,5	3139	0,78
	Average volume	0,87
	Deviation	0,38

Table D.2: Initial Y-stage offset positioning error for a stage speed of 2 [m/s] and an acceleration of 2 [m/s^2].

Test	Gap height [μm]	Calculated offset Calculator V1 [μm]	Actual offset by Y-stage [μm]	Offset difference [μm]
1	55	2,42	4,64	2,22
2	60,7	2,67	4,53	1,86
3	62	2,73	5,07	2,35
4	65	2,86	2,95	0,09
5	100,3	4,41	6,16	1,75
6	114,2	5,02	6,96	1,94
			Average offset difference	**1,70**
			Standard deviation	**0,82**

Table D.3: Overview of the y-stage offset error results, showing the calculated offset, the provided offset, and the offset positioning error.

Test	Gap height[μm]	Calculated offset [μm]	Actual offset [μm]	Offset error [μm]
1	50	5,95	7,24	-1,30
2	50	5,94	5,80	0,13
3	75	5,41	4,14	1,27
4	75	5,29	4,75	0,54
5	100	6,31	6,50	-0,19
6	100	6,89	6,98	-0,09
7	125	5,27	5,75	-0,48
8	125	5,24	4,34	0,89
9	150	5,22	4,68	0,54
10	150	5,22	5,23	-0,01
			Average offset error	**0,12**
			Standard deviation	**0,73**

Table D.4: Gather data about the relationship between the gap height, arc length, and drop volume.

Gap Height [μm]	Arc length [mm]	Drop volume [μL]
50	0,86	0,70
50	0,75	0,29
50	0,88	1,51
50	0,84	0,60
75	0,88	0,84
75	0,81	1,05
75	0,70	0,93
100	0,77	1,74
100	0,65	0,65
100	0,74	1,66
125	0,83	1,08
125	0,76	1,36
125	0,84	1,26
150	1,01	2,25
150	0,88	0,97
150	0,93	1,45
175	0,76	0,45
175	0,70	0,69
175	0,56	0,34
200	0,76	0,79
200	0,63	0,37
200	0,73	0,78

E

Dispensing requirement information

The adhesive volume influences the shrinkage. Figure E.1 shows the calculation error versus the arc length. If the arc length surpasses its upper boundary, this suggests an increase in adhesive volume, as illustrated in Figure E.2. In such cases, the adhesive shrinkage-induced component y-shift exceeds the prediction made by the shrinkage prediction model due to a more pronounced negative calculation error. If the arc length falls below its lower boundary, it suggests a reduction in adhesive volume. Consequently, there is less shrinkage observed compared to what is predicted by the shrinkage prediction model. This discrepancy occurs because the calculation error shifts toward a more positive direction, influencing the accuracy of the prediction.

Based on the observed behavior in the test strategy results, it is evident that the volume significantly influences the optical component displacements induced by adhesive shrinkage. Therefore a dispensing method, capable of dispensing an accurate volume should be implemented, enhancing the accuracy of the compensation prediction. A volume accuracy of 0.1[μL] is sufficiently precise for the adhesive bonding strategy. According to the trend line in Figure B.1, this deviation in adhesive volume would result in an estimated shrinkage calculation error of 0.5 μm. When changing the adhesive volume, additional tests should be conducted for this specific volume under varying gap heights as it would change the shrinkage prediction trend line.

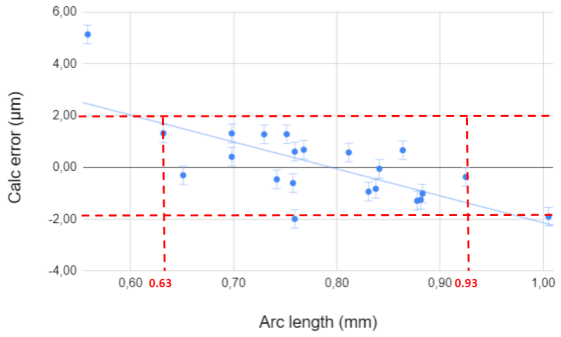

Figure E.1: Scatter plot showing the relationship between the shrinkage prediction error and the arc length.

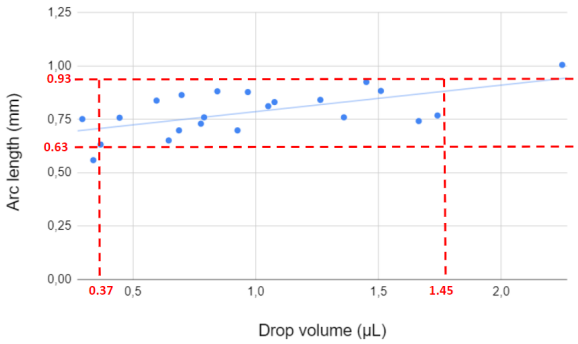

Figure E.2: Scatter plot showing the relationship between the arc length and the dispensed drop volume.

References

[1] Guangyao Li, Zhendong Guo, and Sung-Liang Chen. “Miniature probe for forward-view wide-field optical-resolution photoacoustic endoscopy”. In: *IEEE Sensors Journal* 19.3 (2018), pp. 909–916.

[2] Xianjin Dai et al. “Miniature probe integrating optical-resolution photoacoustic microscopy, optical coherence tomography, and ultrasound imaging: proof-of-concept”. In: *Optics letters* 40.12 (2015), pp. 2921–2924.

[3] Xianjin Dai et al. “Miniature endoscope for multimodal imaging”. In: *Acs Photonics* 4.1 (2017), pp. 174–180.

[4] Antonello Forgione and Salman Yousuf Guraya. “Advanced endoscopic imaging technologies for in vivo cytological examination of gastrointestinal tract lesions: State of the art and proposal for proper clinical application”. In: *Journal of Microscopy and Ultrastructure* 1.3 (2013), pp. 65–75.

[5] Tianrui Zhao, Lei Su, and Wenfeng Xia. “Optical ultrasound generation and detection for intravascular imaging: a review”. In: *Journal of healthcare engineering* 2018 (2018).

[6] Michalina J Gora et al. “Endoscopic optical coherence tomography: technologies and clinical applications”. In: *Biomedical optics express* 8.5 (2017), pp. 2405–2444.

[7] B.E de Vries. “Possibilities of a generic assembly method for miniaturized endoscopic probes”. In: *TU Delft ME-HTE* 1 (2023), pp. 20–22.

[8] Xuanrong Ji et al. “Intravascular confocal photoacoustic endoscope with dual-element ultrasonic transducer”. In: *Optics express* 23.7 (2015), pp. 9130–9136.

[9] Tianshi Wang et al. “Intravascular optical coherence tomography imaging at 3200 frames per second”. In: *Optics letters* 38.10 (2013), pp. 1715–1717.

[10] Yingchun Cao et al. “High-sensitivity intravascular photoacoustic imaging of lipid–laden plaque with a collinear catheter design”. In: *Scientific reports* 6.1 (2016), p. 25236.

[11] CS Premachandran et al. “Design, fabrication, and assembly of an optical biosensor probe package for OCT (Optical Coherence Tomography) application”. In: *IEEE transactions on advanced packaging* 32.2 (2009), pp. 417–422.

[12] Barbara de Vries. “Optical alignment strategies for assembly of endoscopic probes”. In: (2024).

[13] SW Ricky Lee and Chi Chuen Lo. “Passive Alignment of Optical Fibers in V-grooves with Low Viscosity Epoxy Flow”. In: *Micro-and Opto-Electronic Materials and Structures: Physics, Mechanics, Design, Reliability, Packaging*. Springer, 2007, B151–B173.

[14] Pieter-Bas de Potter. “Exploring techniques for flexible micro-assembly and micro-joining in precision engineering”. Literature review”. 2024.

[15] Alessandra Vitale, Giuseppe Trusiano, and Roberta Bongiovanni. “UV-Curing of Adhesives: A Critical Review”. In: *Progress in Adhesion and Adhesives* 3 (2018), pp. 101–154.

[16] Wojciech Lewoczko-Adamczyk, Sebastian Marx, and Henning Schröder. “Shrinkage Measurements of UV-Curable Adhesives: An elegant method based on a laser distance sensor for in-situ measurements of the polymerization shrinkage”. In: *Optik & Photonik* 12.4 (2017), pp. 41–43.

[17] Pugazhenthan Thangaraju and Shoban Babu Varthya. “ISO 10993: biological evaluation of medical devices”. In: *Medical device guidelines and regulations handbook*. Springer, 2022, pp. 163–187.

[18] Fernanda de Carvalho Panzeri Pires de Souza et al. “Polymerization shrinkage stress of composites photoactivated by different light sources”. In: *Brazilian dental journal* 20 (2009), pp. 319–324.

[19] Jialin Zhang et al. “Adaptive pixel-super-resolved lensfree holography for wide-field on-chip microscopy”. In: *arXiv preprint arXiv:1706.04941* (2017).

[20] AJ Hudson et al. “Optical measurements of shrinkage in UV-cured adhesives”. In: *J. Electron. Packag.* 124.4 (2002), pp. 352–354.

[21] *Commercial Quality Windows, Circular, G1 Commercial Grade Fused Quartz — escooptics.com*. https://escooptics.com/products/windows-commercial-quality-circular-g1-commercial-grade-fused-quartz?variant=14978622723. [Accessed 03-02-2024].

[22] Adam Chafaï et al. “Two-dimensional modelling of transient capillary driven damped micro-oscillations and self-alignment of objects in microassembly”. In: *Journal of Fluid Mechanics* 910 (2021), A6.

[23] Jiawen Li et al. “Miniature integrated optical coherence tomography (OCT)-ultrasound (US) probe for intravascular imaging”. In: *Photonic Therapeutics and Diagnostics VIII*. Vol. 8207. SPIE. 2012, pp. 550–556.

[24] Tobias Müller et al. “Strategies for precision adhesive bonding of micro-optical systems”. In: *Components and Packaging for Laser Systems*. Vol. 9346. Spie. 2015, pp. 88–95.

[25] Guiling Deng et al. “A piezoelectric jetting dispenser with a pin joint”. In: *Optik* 175 (2018), pp. 163–171.

[26] Huifang Liu et al. “A pL-fL grade micro-dispensing by pipetting needle glue liquid transfer”. In: *AIP Advances* 11.6 (2021).

[27] Matthijs HM van Gastel, PCJ Nick Rosielle, and Maarten Steinbuch. “A concept for accurate edge-coupled multi-fiber photonic interconnects”. In: *Journal of Lightwave Technology* 37.4 (2019), pp. 1374–1380.